NEAR EAST UNIVERSITY

Faculty of Engineering

Department of Electrical & Electronic Engineering

BISTATIC RADAR

Graduation Project
EE 400

Mohammed Alshaikhkhalil
20022096

Supervisor: assoc. Prof. Dr. Sameer Ikhdair

Nicosia - 2005

ABSTRACT

We had thought to do our work on the biostatic radar, and then we searched for the important parts on this subject since the biostatic radar and the radar in general is one of the most common parts in communication system and both civil and military uses.

Biostatic radar systems have been studied and built since the earliest days of radar. They have the advantages that the receivers are passive, and hence undetectable. The receiving systems are also potentially simple and cheap. Biostatic radar may have a counter-stealth capability, since target shaping to reduce monostatic RCS will in general not reduce the biostatic RCS. In spite of those advantages, rather few biostatic radar systems have got past the 'technology demonstrator' phase. It has also been remarked that activity in biostatic radar tends to vary on a period of approximately fifteen years, and that currently we are at a peak of that cycle; there is particular current interest in passive coherent location (PCL) techniques, using broadcast and communications signals as 'illuminators of opportunity'. Keywords: biostatic radar, multistatic radar, passive coherent location. We have recently extended the passive radar technique to permit interferometer observation of ionospheric irregularities. We discuss the implementation of a passive radar interferometer at VHF frequencies and show observations of field-aligned irregularities in the high latitude E-region ionosphere. The interferometer achieves very fine azimuthally resolution (as fine as 0:1, or 2 km at a range of 1000 km); thus, we can form two dimensional spatial images of the target volume. Many E-region scatterers are compact, with transverse extent no greater than 15 km; this is significantly smaller than the beam width of most coherent radars. By tracking interferometric position, we can estimate the transverse drift of the scattering region. By coupling this information with the line of sight Doppler shift and using the dispersion relation for meter scale irregularities, we estimate electric fields and velocity shears within the scattering volume.

CONTENTS

ACKNOWLEDGMENTS i

ABSTRACT ii

TABLE OF CONTENTS iii

INTRODUCTION 1

1. TYPES OF RADAR 3

1.1 Different Types of Radar 3

1.1.1 Doppler Radar 3

1.1.2 Dual Wavelength Polarized Radar 3

1.1.3. Bistatic Radar 4

1.2 Principles of Radar 5

1.3 Radar Bands 7

1.4 Hardware of Radar 8

1.5 The Radar Equation 11

1.6 Basic Radar Concepts 14

1.7 Introduction to SAR: A Signal Processing Viewpo 15

1.7.1 Automatic Target Recognition using SAR 15

1.8 Radar Cross Section 16

1.9 Theory, Applications, and Advanced Techniques 16

1.10 Pulse Compression in Radar Systems 17

1.11 Different Radar System Set-ups 18

1.12 Uses of Radar 18

1.13 Differences and similarities between radar and communication systems 19

1.14 Noise in Radar Systems 20

1.15 Electronic Warfare and Radar Systems 20

2. BISTATIC AND MULTISTATIC RADAR 21

2.1 Introduction 21

2.2 Properties of Bistatic Radar 22

2.2.1 Bistatic Radar Geometry 22

2.2.2 Bistatic Radar Cross Section 24

2.2.3 Forward scatter 25
2.2.4 Bistatic Clutter 26
2.2.5 The Ambiguity Function for Bistatic Radar 26

2.3 Applications of Multistatic Radar 27
2.3.1 Basaltic Radar on Mars Express 27

3. EXAMPLES OF PASSIVE COHERENT SYSTEM 29

3.1 Passive Coherent Location 29
3.2 Examples of System 34
3.2.1 Amateur Radio Forward Scatter Experiment 34
3.2.2 Non-co-operative Radar Illuminators 34
3.2.3 Television-based Bistatic Radar 36
3.2.4 TV-based Forward Scatter System 37
3.2.5 The Manastash Ridge Radar 38
3.2.6 Silent Sentry 39

4. PASSIVE COHERENT SCATTER RADAR INTERFEROMETER IMPLEMENTAION, OBSERVATIONS, AND ANALYSIS 40

4.1 Introduction 40
4.2 Implementation 42
4.2.1 The Interferometer Cross-Correlation Estimator 44
4.3 Results 50
4.3.1 Two-Dimensional Images 52
4.3.2 Velocity and Electric Field Measurements 54
4.4 Analysis of Data Products 56
4.5 Summary 58
4.6 Conclusions 59

REFERENCES 60

INTRODUCTION

The word radar means a method of detecting distant objects and determining their position, velocity, or other characteristics by analysis of very high frequency radio waves reflected from their surfaces.

The equipment used in such detection Radar is an acronym for radio detection and ranging. It is a system used to detect, range (determine the distance of), and map objects such as aircraft and rain. Strong radio waves are transmitted, and a receiver listens for any echoes. By analysing the reflected signal, the reflector can be located, and sometimes identified. Although the amount of signal returned is tiny, radio signals can easily be detected and amplified. Radar radio waves can be easily generated at any desired strength, detected at even tiny powers, and then amplified many times.

Thus radar is suited to detecting objects at very large ranges where other reflections, like sound or visible light, would be too weak to detect. Primary radar is a radio determination system based on the comparison of reference signals with radio signals reflected from the position to be determined. The secondary radar is a radio determination system based on the comparison of reference signals with radio signals retransmitted from the position to be determined. [NTIA] [RR] Note: An example of secondary radar is the transponder-based surveillance of aircraft. Synonym secondary surveillance radar.

Weather radar has made many improvements in the last 10 years. There are more improvements on the way. All of the radars of the past and present work off the same basic principle: the radar equation below.

The basic concept of weather radar works off of the idea of a reflection of energy. The radar sends out a signal, as seen to the right, and the signal is then reflected back to the radar. The stronger that the reflected signal is the larger the particle.

Biostatic radar systems have been studied and built since the earliest days of radar. As an early example, the Germans used the British Chain Home radars as illuminators for their Klein Heidelberg bistatic system. Bistatic radars have some obvious advantages. The receiving systems are passive, and hence undetectable. The receiving systems are also potentially simple and cheap. Bistatic radar may also have a counter stealth capability, since target shaping to reduce target monostatic RCS will in general not reduce the biostatic RCS.

Furthermore, biostatic radar systems can utilize VHF and UHF broadcast and communications signals as 'illuminators of opportunity', at which frequencies target stealth treatment is likely to be less effective.

Biostatic systems have some disadvantages. The geometry is more complicated than that of monostatic systems. It is necessary to provide some form of synchronization between transmitter and receiver, in respect of transmitter azimuth angle, instant of pulse transmission, and (for coherent processing) transmit signal phase. Receivers which use transmitters which scan in azimuth will probably have to utilize 'pulse chasing' processing.

Over the years a number of biostatic radar systems have been built and evaluated. However, rather few have progressed beyond the 'technology demonstrator' phase. Willis [33] has remarked that interest in biostatic radar tends to vary on a period of approximately fifteen years, and that currently we
are at a peak of that cycle.

The purpose of this paper is therefore to present a review of the properties and current developments in biostatic and multistatic radar, with particular emphasis on passive coherent location using broadcast or communications transmissions.

Chapter one is primary concerned with definitions and related terminology. There is an explanation of radar and structure with some equation and figures and the types of radar and the radar equation as well.

Chapter two give information about the multistatic and bistatic radar considering the structure and the functions. Chapter three presents examples of passive coherent location and the use of broadcast or communications signals as 'illuminators of opportunity'. Finally in chapter four we give applications summary and conclusion of the project.

CHAPTER ONE

TYPES OF RADAR

1.1 Different Types of Radar

1.1.1 Doppler Radar:

Dopplerizing existing radar adds the capability of measuring wind direction and speed by measuring the Doppler effect. The radar measures what is called radial velocity. This is the component of the wind going either toward or away from the radar. There are currently two different types of radar that are being experimented with. The first type that is in the final stages of development is dual-polarized radar. The other that is being worked on is bistatic radar.

1.1.2 Dual Wavelength Polarized Radar:

This is actually an upgrade to the existing radar principle like the addition of Doppler was. Since the current WSR-88D's is to be upgraded to this type of radar by the year 2005, it would be helpful to take a look at what this upgrade will do for us. With dual-polarization, there is the use of two or more wavelengths. This permits the extraction of additional information about the different meteorological targets. The radar echo of the targets changes with wavelength. The reflectivity of small targets, targets that are much smaller than the radar wavelength, is similar at two different wavelengths. For large targets like wet snowflakes and hail, the reflectivity differs. This helps solve the problem mentioned above referring to the raindrop size and its reflectivity. Size of the particle will be something that the radar can determine. This will allow for more information on the storm processes, and help forecast and warn on storms better. Also, with the dual-polarization, there is a dual-wavelength signature for large hail. Currently in on-going research, this type of radar can see more than just rain in the clouds. Dual-polarized radar can determine the following parts of a thunderstorm: Cloud Drops, Drizzle, Light Rain, Moderate Rain, Heavy Rain, Hail, Rain/Hail, Graupel/Small Hail, Graupel/Rain, Dry Snow, Wet Snow, Ice Crystals, Irregular Ice Crystals, Super-Cooled Liquid Water Droplets, and Insects.

1.1.3. Biostatic Radar

This is probably the newest instrument on the horizon for radar since it was created in 1994. In the past, a problem occurred in detecting the wind structure of a thunderstorm with a single Doppler radar. This was a problem

Figure 1.1. Structure of radar

Because if the winds were flowing perpendicular to the radar beam, it could not resolve which direction they were flowing from. This problem is corrected with bistatic radars. In a bistatic system, there is at least one bistatic receiver and one single traditional monostatic weather radar. In this system, the weather radar transmits a narrow beam and receives the backscattered radiation. At the same time, one or more passive bistatic receivers recover some of the other scattered radiation. Since this gives multiple angles on the wind, many components of the wind can be measured simultaneously. This creates the possibility of directly measuring 3-D winds with a single radar system. There currently is only one bistatic radar network set up in the world. That network is set up around the Montreal airport in Canada. The preliminary results have been very promising, especially in areas like airports that require a good understanding of wind flow. An example of the data is below. One can see below in the data the direction and speed of the winds. This solves the problem that single dopplers have. Single dopplers can only see wind direction toward or away from the radar.

1.2 Principles of Radar

Weather radar has made many improvements in the last 10 years. There are more improvements on the way. All of the radars of the past and present work off the same basic principle: the radar equation below.

The basic concept of weather radar works off of the idea of a reflection of energy. The radar sends out a signal, as seen to the right, and the signal is then reflected back to the radar. The stronger that the reflected signal is the larger the particle.

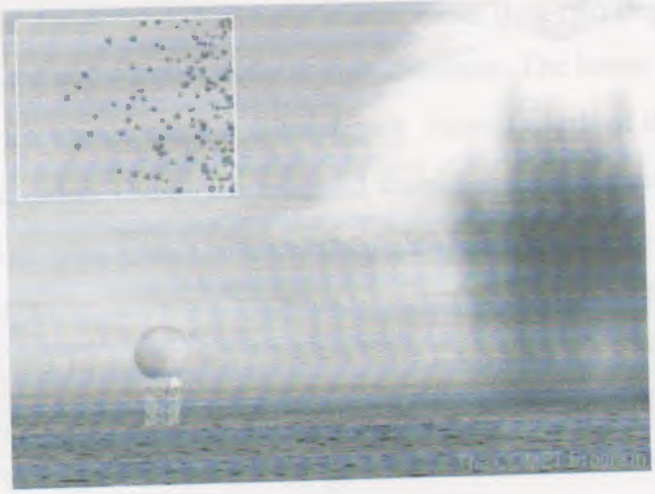

Figure 1.2 Weather radar

At the heart of the principle of radar is the radar equation.

$$P_r = \frac{P_t G^2 \theta H \pi^3 K^2 L}{1024 (\ln 2) \lambda^2} \times \frac{Z}{R^2} \quad (1.1)$$

This equation involves variables that are either known or are directly measured. There is only one value that is missing, but it can be solved for mathematically. Below is the list of variables, what they are, and how they are measured. L^2 Where, p_r : Average power returned to the radar from a target. The radar sends up to 25 pulses and then measures the average power that is received in those returns. The radar uses multiple pulses since the power returned by a meteorological target varies from pulse to pulse. This is an unknown value of the radar, but it is one that is directly calculated. p_t : Peak power transmitted by the radar. This is a known value of the radar. It is important to know because the average power returned is directly related to the transmitted power. G : Antenna gain of the radar. This is a known value of the radar. This is a measure of the antenna's ability to focus outgoing energy into the beam. The power received from a given target is directly related to the square of the antenna gain. θ : Angular beamwidth of the radar. This is a known value of the radar. Through the Probert-Jones equation it can be learned that the return power is directly related to the square of the angular beamwidth. The problem becomes that the assumption of the equation is that precipitation fills the beam for radars with beams wider than two degrees. It is also an invalid assumption for any weather radar at long distances. The lower resolution at great distances is called the aspect ratio problem. H is a Pulse Length of the radar. This is a known value of the radar. The power received from a meteorological target is directly related to the pulse length. K is a physical constant. This is a known value of the radar. This constant relies on the dielectric constant of water. This is an assumption that has to be made, but also can cause some problems. The dielectric constant of water is near one, meaning it has a good reflectivity. The problem occurs when you have meteorological targets that do not share that reflectivity. Some examples of this are snow and dry hail since their constants are around 0.2. L is the loss factor of the radar. This is a value that is calculated to compensate for attenuation by precipitation, atmospheric gases, and receiver detection limitations. The attenuation by precipitation is a function of precipitation intensity and wavelength. For atmospheric gases, it is a function of elevation angle, range, and wavelength. Since all of these accounts for a 2dB loss, all signals are strengthened by 2 dB. λ is the wavelength of the transmitted energy. This is a known value of the radar. The amount of power returned from a precipitation target is inversely since the short wavelengths are subject to significant attenuation. The longer the wavelength, the less attenuation caused by precipitate. Z is the reflectivity factor of the precipitate. This is the value that is solved for mathematically by the radar. The number of drops and the size of the drops affect this value. This value can cause problems because the radar cannot determine the size of the precipitate. The size is important since the reflectivity factor of a precipitation target is determined by raising each drop diameter in the sample volume to the sixth power and then summing all those values together. A ¼" drop reflects the same amount of energy as 64 1/8" drops even though there is 729 times more liquid in the 1/8" drops. R is the target range of the precipitate. This value can be calculated by measuring the time it takes the signal to return. The range is important since the average power return from a target is inversely related to the square of its range from the radar. The radar has to normalize the power returned to compensate for the range attenuation. Using a relationship between Z and R, an estimate of rainfall can be achieved. A base equation that can be used to do this is Z=200*R^1.6. This equation can be modified at the user's request to a better fitting equation for the day or the area.

1.3 Radar Bands

Doppler radar can be divided into several different categories according to the wavelength of the radar. The different bands are L, S, C, X, K. The names of the radars originate from the days of WWII. L band radars operate on a wavelength of 15-30 cm and a frequency of 1-2 GHz. L band radars are mostly used for clear air turbulence studies. S band radars operate on a wavelength of 8-15 cm and a frequency of 2-4 GHz. Because of the wavelength and frequency, S band radars are not easily attenuated. This makes them useful for near and far range weather observation. The National Weather Service (NWS) uses S band radars on a wavelength of just over 10 cm. The drawback to this band of radar is that it requires a large antenna dish and a large motor to power it. It is not uncommon for a S band dish to exceed 25 feet in size. C band radars operate on a wavelength of 4-8 cm and a frequency of 4-8 GHz. Because of the wavelength and frequency, the dish size does not need to be very large. This makes C band radars affordable for TV stations. The signal is more easily attenuated, so this type of radar is best used for short range weather observation. Also, due to the small size of the radar, it can therefore be portable like the University of Oklahoma's Doppler on Wheels. (DOW)

The frequency allows C band radars to create a smaller beam width using a smaller dish. C band radars also do not require as much power as S band radar. The NWS transmits at 750,000 watts of power for their S band, where as a private TV station such as KCCI-TV in Des Moines only broadcasts at 270,000 watts of power with their C band radar. X band radars operate on a wavelength of 2.5-4 cm and a frequency of 8-12 GHz. Because of the smaller wavelength, the X band radar is more sensitive and can detect smaller particles. These radars are used for studies on cloud development because they can detect the tiny water particles and also used to detect light precipitation such as snow.. X band radars also attenuate very easily, so they are used for only very short range weather observation. Most major airplanes are equipped with X band radar to pick up turbulence and other weather phenomenon. This band is also shared with some police speed radars and some space radars. K band radars operate on a wavelength of .75-1.2 cm or 1.7-2.5 cm and a corresponding frequency of 27-40 GHz and 12-18 GHz. This band is split down the middle due to a strong absorption line in water vapor. This band is similar to the X band but is just more sensitive. This band also shares space with police radars

1.4 Hardware of Radar

There is a lot of hardware that is necessary for a radar to run, here is a brief look at some of the main components required to run a National Weather Service (NWS) WSR-88D NexRad radar. The most seen component of a radar is the actual dome itself. Especially with S band radars, see the bands section, a large dome is needed. Since this dome can easily be over 30 feet in height and on top of a tower over 100 feet in height, it can be visible from long distances. The dome

Figure 1.3 Hardware of Radar

Essentially just houses and protects the radar dish. It is made of a material that allows the signal to leave through it and also return through it. Inside that dome is the dish itself.

Figure 1.4 The dish inside the dome

The main purpose of the dish is to focus the transmitted power into a small beam and also to listen and collect the returned signal. More information about dish sizes can also be found in the bands section. In a nutshell, that is essentially what radar's dish does. That visible part is really just a small part of what actually makes the radar work. There are three components in WSR-88 D radar besides the dish and tower. These are the Radar Data Acquisition (RDA), the Radar Product Generator (RPG), and finally the Principal User Processor. (PUP) RDA - The radar data acquisition unit is what houses the actual transmitter and the receiver. The transmitter sends out multiple pulses every second. Between those pulses, the receiver receives the reflected energy from the pulse. Since precipitation is moving and every return signal is different, it reads over 20 pulses per second and sends that data on to the RPG. RPG - The radar product generator receives the information from the receiver. It takes the 20 or more pulses that the receiver received in one second and averages them together. After the RPG gets the information from one volume scan, or one rotation of the radar, it creates the products that we see on TV or the Internet. Some of these products are the reflectivity of the precipitation and also the velocities of the precipitation calculated using the Doppler Effect. PUP - The principal user processor is the unit that allows for the interface with the radar. This has been in the past the only workstation that allowed a user to access the radar data and control the radar. Now, the NWS is installing AWIPS in all of their offices. This allows anyone in the building to access the radar data. This will aid in monitoring multiple storms and help get warnings issued more quickly.

1.5 The Radar Equation

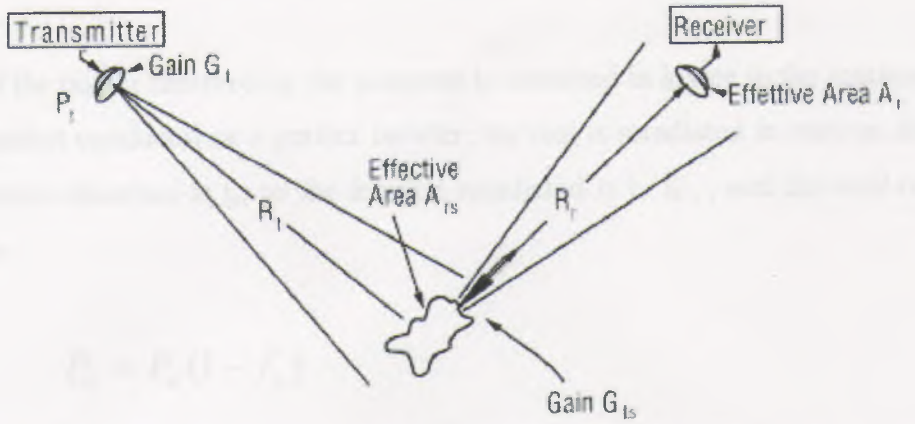

Figure 1.4. The fundamental relation between the characteristic of the radar

The fundamental relation between the characteristics of the radar, the target, and the received signal is called the radar equation. The geometry of scattering from an isolated radar target (scatterer) is shown in the figure, along with the parameters that are involved in the radar equation. When a power P_t is transmitted by an antenna with gain G_t , the power per unit solid angle in the direction of the scatterer is P_t G_t, where thevalue of G_t in that direction is used. At the scatterer,

$$S_{s} = (P_t G_t)\left(\frac{1}{4\pi R^2}\right) \tag{1.2}$$

where S_s is the power density at the scatterer. The spreading loss $\frac{1}{4\pi R^2}$ is the reduction in power density associated with spreading of the power over a sphere of radius R surrounding the antenna. To obtain the total power intercepted by the scatterer, the power density must be multiplied by the effective receiving area of the scatterer:

$$P_{rs} = S_t A_{rs} \tag{1.3}$$

Note that the effective area A_{rs} is not the actual area of the incident beam intercepted by the scatterer, but rather is the effective area; i.e., it is that area of the incident beam from which all power would be removed if one assumed that the power going through all the rest of the beam continued uninterrupted. The actual value of A_{rs} depends on the effectiveness of the scatterer as a receiving antenna.

Some of the power received by the scatterer is absorbed in losses in the scatterer unless it is a perfect conductor or a perfect isolater; the rest is reradiated in various directions. The fraction absorbed is f_a, so the fraction reradiated is 1- f_a , , and the total reradiated power is

$$P_{ts} = P_{ts}(1 - f_a) \tag{1.4}$$

The conduction and displacement currents that flow in the scatterer result in reradiation that has a pattern (like an antenna pattern). Note that the effective receiving area of the scatterer is a function of its orientation relative to the incoming beam, so that A_{rs} in the equation above is understood to apply only for the direction of the incoming beam.

The reradiation pattern may not be the same as the pattern of A_{rs}, and the gain in the direction of the receiver is the relevant value in the reradiation pattern. Thus,

$$S_t = P_{ts} G_{ts} \frac{1}{4\pi R^2} \tag{1.5}$$

where P_{ts} is the total reradiated power, G_{ts} is the gain of the scatterer in the direction of the receiver, and $\frac{1}{4\pi R^2}$ is the spreading factor for the reradiation. Note that a major difference between a communication link and radar scattering is that the communication link has only one spreading factor, whereas the radar has two. Thus, if $R_r = R_t$, the total distance is $2R_t$; for a communication link with this distance, the spreading factor is only: $\frac{1}{4}\left(\frac{1}{4\pi R_t^2}\right)$ whereas for the radar it is: $\left(\frac{1}{4\pi}\right)^2\left(\frac{1}{R_t}\right)^4$ Hence, the spreading loss for a radar is much greater than for a communication link with the same total path length.

The power entering the receiver is

$$P = SA \tag{1.6}$$

where the area A_r is the effective aperture of the receiving antenna, not its actual area. Not only is this a function of direction, but it is also a function of the load impedance the receiver provides to the antenna; for example,P_r would have to be zero if the load were ashort circuit or an open circuit. The factors in the eq. 1 through the eq. 5 may be combined to obtain

$$\begin{aligned} P_t &= \left(P_t G_t\right)\left(\frac{1}{4\pi R_t^2}\right) A_{ts}(1 - f_a) G_{ts}\left(\frac{1}{4\pi R^2}\right) A_t \\ &= \left(\frac{P_t G_t A_t}{(4\pi)^2 R_t^2 R_t^2}\right)\left[A_{ts}(1-f_a) G_{ts}\right] \end{aligned} \tag{1.7}$$

The factors associated with the scatterer are combined in the square brackets. These factors are difficult to measure individually, and their relative contributions are uninteresting to one wishing to know the size of the received radar signal. Hence they are normally combined into one factor, the radar scattering cross section:

$$\sigma = A_{ts}(1-f_a) G_{ts} \tag{1.8}$$

The cross-section s is a function of the directions of the incident wave and the wave toward the receiver, as well as that of the scatterer shape and dielectric properties.

The final form of the radar equation is obtained by rewriting the eq. 6 using the definition of the eq.

$$P_t = \frac{P_t G_t A_t}{(4\pi)^2 R_t^2 R_t^2} \sigma \tag{1.9}$$

The most common situation is that for which receiving and transmitting locations are the same, so that the transmitter and receiver distances are the same. Almost as common is the use of the same antenna for transmitting and receiving, so the gains and effective apertures are the same, that is:

$$R_t = R_r = R$$

$$G_t = G_r = G$$

$$A_t = A_r = A$$

Since the effective area of an antenna is related to its gain by:

$$A = \frac{\lambda^2 G}{4\pi} \tag{1.10}$$

we may rewrite the radar equation (eq. 1.9) as

$$P = \frac{P_t G^2 \lambda^2 \sigma}{(4\pi)^3 R^4} = \frac{P_t A^2 \sigma}{4\pi \lambda^2 R^4} \tag{1.11}$$

where two forms are given, one in terms of the antenna gain and the other in terms of the antenna area. The radar equations (eq. 1.9 and eq. 1.11) are general equations for both point and area targets. That is, the scattering cross-section s is not defined in terms of any characteristic of a target type, but rather is the scattering cross-section of a particular target. The form given in the equation 1.11 is for the so-called monostatic radar, and that in eq. 1.9 is for bistatic radar, although it also applies for monostatic radar when the conditions for R, G, A given above are satisfied.

1.6 Basic Radar Concepts

Basic Radar Concepts is a course in the basic fundamental principles of modern radar technology. This course is intended to impart to the student a basic, high-level, understanding of today's modern radar technology in simple, easy-to-under-stand terms. The two instructors, Bill Holm and Jim Scheer, have a vast level of experience in presentation of radar-related short course material, and have, over the years, developed an understanding of how to best present special topics (e.g. propagation phenomena, Nyquist sampling issues, use of decibel (dB) nomenclature, probability density functions, etc.) using easy-to-interpret everyday situations as examples. Topics include: Introduction to Radar — definitions, classes of radars, radar range equation, radar cross section, detection process, and design considerations, and Basic Elements of the Radar System — transmitters, receivers, antennas (including phased arrays) and signal processing and processors

1.7 Introduction to SAR: A Signal Processing Viewpo

Synthetic aperture radar (SAR) is a microwave system capable of synthesizing imagery having extraordinary resolution by processing radar data collected from a single sensor moved to different spatial locations. This tutorial focuses on developing the fundamental mathematical ideas underlying both strip-map and spotlight-mode SAR. The signal processing aspects of SAR are stressed and an understanding of the image formation process is gained, beginning with the original scene reflectivity and ending with the final image. For strip-map SAR, three image reconstruction methods are described: correlation based, chirp scaling, and w-k. For spotlight-mode SAR, we concentrate on the polar-format approach. Using theorems from 3-D computer tomography, the relationship of a 2-D SAR image to the true 3-D scene is explained. Also, SAR interferometry is developed for topographic mapping, and the phase unwrapping problem is discussed. When imaging 3-D objects having irregular shapes, interferometric SAR suffers from layover, where various parts of the 3-D object are collapsed into 2-D. A new method of radar imaging of complex 3-D objects is described, where the imaging problem is converted into a high-resolution spectral estimation problem. Reconstructions of military targets are shown using simulated radar data generated by XPATCH

1.7.1 Automatic Target Recognition using SAR

This tutorial on Automatic Target Recognition (ATR) using Synthetic Aperture Radar (SAR) imagery focuses on two main areas of research: (1) SAR ATR using fully polarimetric data and (2) SAR ATR using superresolution image processing. In part 1 of the tutorial we describe a fully polarimetric Ka -band SAR sensor, and we develop various techniques, including the polarimetric whitening filter (PWF) and the polarimetric matched filter (PMF), for optimum processing of the fully polarimetric data. A complete end-to-end target recognition system is developed, and performance results versus resolution and polarization are summarized. In part 2 of the tutorial, various superresolution processing algorithms applied to SAR data are described, and for each algorithm the improvement in ATR performance is quantified. Recognition performance results are presented for a 20-target classifier, and lessons learned from extensive SAR ATR evaluations conducted at MIT Lincoln Laboratory are summarized.

Additional ATR topics to be presented include: target recogni-tion performance comparisons using 1-D high range resolution (HRR) profile classifiers versus 2-D SAR classifiers; model-based classifier performance; combined polarimetric/ superresolution processing; and low frequency foliage penetration (FOPEN) SAR target detection and discrimination.

1.8 Radar Cross Section

This tutorial will cover the following radar cross section (RCS) topics: An Overview of Stealth; RCS Scattering Mechanisms; RCS Prediction Methods; and RCS Scattering Center Visualization. An Overview of Stealth includes a top-level description of the basic approaches to stealth design and considerations starting with the notion of threat sectors. The four basic approaches to RCS reduction will be reviewed with emphasis on shaping. RCS Scattering Mechanisms will highlight the physical processes by which incident electromagnetic energy is re-radiated. Included will be a consideration of scattering centers using a visual approach. Scattering mechanisms to be discussed include: specular, multiple bounce, end region returns (which are responsible for pattern side lobes), edge diffraction, surface traveling/edge/creeping waves, and surface imperfection scattering. RCS Prediction Methods will overview some of the basic approaches used to compute mono- and bistatic scattering. Topics for consideration include Physical Optics and Physical Theory of Diffraction for large targets and Method of Mo-ments (MOM) codes for moderate sized targets. RCS Scattering Center Visualization includes image animations of scattering centers from measured and computed data. The bi-static k-space imaging approach for analytical computations without a frequency sweep will be reviewed.

1.9 Theory, Applications, and Advanced Techniques

This tutorial is designed to provide a firm grounding in both the underlying theory of optimum and adaptive array processing, as well as an understanding of the key practical challenges facing real-world implementations. After introducing the motivation and theory of 1D, 2D (i.e., space-time adaptive processing—STAP), and 3D STAP, the course focuses on practical implementation issues. Particular emphasis is placed on those real-world factors that can have a significantly deleterious effect on performance, such as interference heterogeneity/nonstationarity, and subspace leakage (i.e., internal clutter motion, nonlinear array geometries, transmitter/ receiver instabilities, etc.). The latest techniques, drawn from up to the minute research for combating these effects, are surveyed and contrasted.

1.10 Pulse Compression in Radar Systems

The principles, motivations, and terminology related to radar pulse compression are presented with an emphasis on obtaining a fundamental understanding of the concepts and techniques involved. The lecture contains an in-depth discussion of specific pulse compression techniques based on frequency, phase, and hybrid modulation schemes. Frequency modulation techniques include linear and non-linear frequency modulation, Stretch, and stepped-frequency waveforms. Particular phase modulation techniques reviewed in the course include Barker, MPS, pseudorandom, Golay, Welti, Frank, and P4 codes, and the 'concatenation' of these codes for the construction of long code-filter designs. The course closes with a discussion of innovative mismatch filtering techniques and the analysis and evaluation of pulse compression schemes based on application of the radar ambiguity function. Dr. Cohen seeks to both inform and entertain his students in an atmosphere conducive to learning. Extensive references and a PDF file of the entire tutorial are provided to ensure that the student is well-equipped to translate attendance at the tutorial into an ability to apply the material on the job.

1.11 Different Radar System Set-ups

Most of the radar systems have the transmitter and receiver in the same location, momostatic radar.

There are however systems in use where the receiver and the transmitter are in different locations, this is called the biostatic radar, and cases where there are multiple receivers and transmitter is called multistatic radar .

There are cases where the transmitted signal is not of the radio spectrum , such as sonar, Which is used for under water detecting, here the transmitted wave is in acoustic spectrum . Acoustic systems are also sometimes used for atmosphering sensing .

1.12 Uses of Radar

Radar is used to gain information about the surrounding areas. For example what is the weather like, is there a aircraft, ships, tank etc approaching. Like most things there are specialist radar systems that perform different tasks. These types of radar called multi-mode radar systems.

Multi-mode systems using don't perform as well as their single-mode counterparts in any particular task abut are used when space is at a premium, like in an aircraft. The information gathered by radar systems can be used to control other systems directly, like autopilots, automated weaponry, or can be used to help human supervisors to control aircraft and the like. The E-3 AWAS (Airborne Warning and Control System) is an example of an airborne supervisory role of radar. There are many other applications of radar systems.

Figure 1.5 Radar on an aircraft

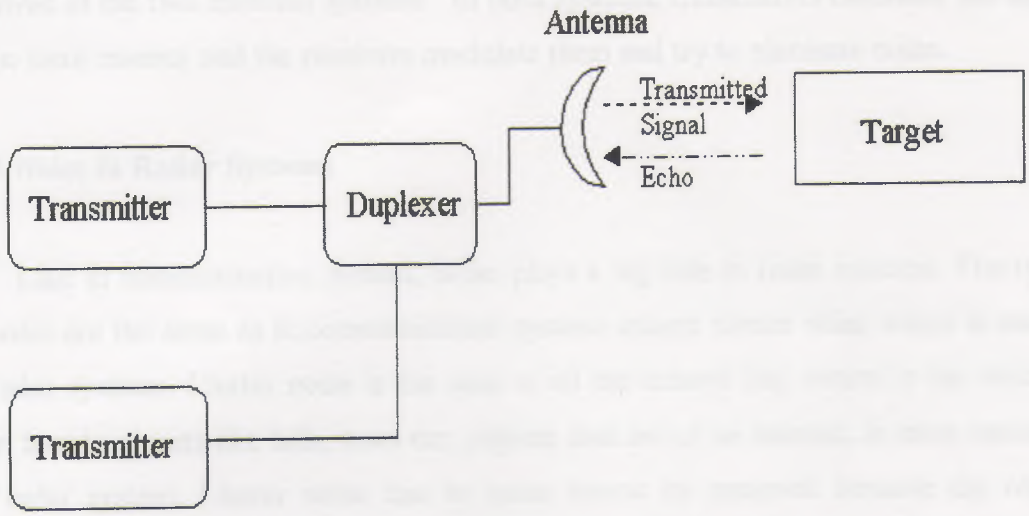

Figure 1.6 The basic block diagram of a monostatic radar system.

Monostatic means that the receiver and transmitter are in same place.

1.13 Differences and similarities between radar and communication systems

The main difference between the communications system and the radar system is that in the radar system the information doesn't originate at the transmitter. The information originates at the target. Radar and communication system have a lot in common. Signals that are transmitted by each system are very similar. The processing of these signals, specially to reduce noise are very similar and so not much detail will be given here as it assume the reader has a good understanding of communication systems.
Differences lie in the variety of signals used by the two systems. The signals used in radar systems are a subset of those used in communication systems. The name of the radar is sometimes taken from the type of signal they used. The signal used is varied depending on what information is to be extracted from the echo produced by the target. If foe example the distance to the target is only important then the pulse would be used

as this allows the precise point to point reference. A continuous signal wave a oure cosine may be used in situations where the frequency shift caused by the Doppler effect needs to be measured to determine the velocity of the target.

As for the similarities according to the processing signals, here the similarities are overwhelming with the only differences being the power and the frequency range involved in the two different systems. In both systems, transmitters modulate the signal in the same manner and the receivers modulate them and try to eliminate noise.

1.14 Noise in Radar Systems

Like in communication system, noise plays a big role in radar systems. The types of noise are the same as in communication systems except clutter noise which is unique to radar systems. Clutter noise is the sum of all the echoes that return to the receiver from terrain objects like hills, trees etc, objects that are of no interest, in most cases, to the radar system. Clutter noise can to some extent by removed because the object producing the unwanted echo is stationary and this leads to the ability to detect and ignore them. The same techniques are used in radar systems to reduce the influences of noise that are used in communication systems.

1.15 Electronic Warfare and Radar Systems

Electronic warfare is used both against radar systems and by radar systems. Electronic countermeasure (ECM) techniques are used to decrease the effectiveness of a radar system or the make the radar system make an erroneous measurement of the position and numbers of targets. Electronic counter countermeasures (ECCM) are used in radar systems to reduce the effect that ECM techniques have on the performance of the system.

CHAPTER TWO

BISTATIC AND MULTISTATIC RADAR

2.1 Introduction

Bistatic radar systems have been studied and built since the earliest days of radar. As an early example, the Germans used the British Chain Home radars as illuminators for their Klein Heidelberg bistatic system. Bistatic radars have some obvious advantages. The receiving systems are passive, and hence undetectable. The receiving systems are also potentially simple and cheap. Bistatic radar may also have a counter stealth capability, since target shaping to reduce target monostatic RCS will in general not reduce the bistatic RCS.

Furthermore, bistatic radar systems can utilize VHF and UHF broadcast and communications signals as 'illuminators of opportunity', at which frequencies target stealth treatment is likely to be less effective.

Bistatic systems have some disadvantages. The geometry is more complicated than that of monostatic systems. It is necessary to provide some form of synchronization between transmitter and receiver, in respect of transmitter azimuth angle, instant of pulse transmission, and (for coherent processing) transmit signal phase. Receivers which use transmitters which scan in azimuth will probably have to utilize 'pulse chasing' processing.

Over the years a number of bistatic radar systems have been built and evaluated. However, rather few have progressed beyond the 'technology demonstrator' phase. Willis [33] has remarked that interest in bistatic radar tends to vary on a period of approximately fifteen years, and that currently we are at a peak of that cycle.

The purpose of this paper is therefore to present a review of the properties and current developments in bistatic and multistatic radar, with particular emphasis on passive coherent location using broadcast or communications transmissions.

2.2 Properties of Bistatic Radar

2.2.1 Bistatic Radar Geometry

The properties of bistatic radar have been described in detail by Willis [31, 32] and by Dunsmore [6]. Jackson [17] has analyzed the geometry of bistatic radar systems, and his notation has been widely adopted.

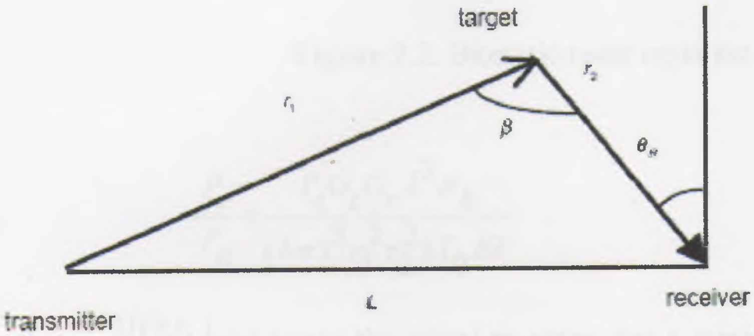

Figure 2.1 bistatic radar geometry

From this:

$$r_2 = \frac{(r_1 + r_2)^2 - L^2}{2(r_1 + r_2 + L\sin\theta_R)} \tag{2.1}$$

Contours of constant bistatic range are ellipses, with transmitter and receiver as the two foci. The bistatic radar equation is derived in the same way as the monostatic radar equation:

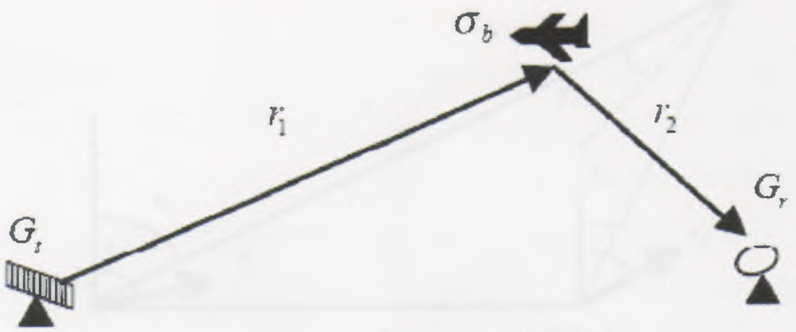

Figure 2.2. Biostatic radar equation

$$\frac{P_r}{P_n} = \frac{P_t G_t G_r \lambda^2 \sigma_b}{(4\pi)^3 r_1^2 r_2^2 k T_0 B F} \tag{2.2}$$

The factor $1/(r_1 r_2)$ and hence the signal-to-noise, has a minimum value for T $r_1 = r_2$. thus the signal-to-noise ratio is highest for targets close to the transmitter or close to the receiver.

Doppler shift depends on the motion of target, transmitter and receiver (Figure 2.2), and in the general case the equations are quite complicated [17, 32].

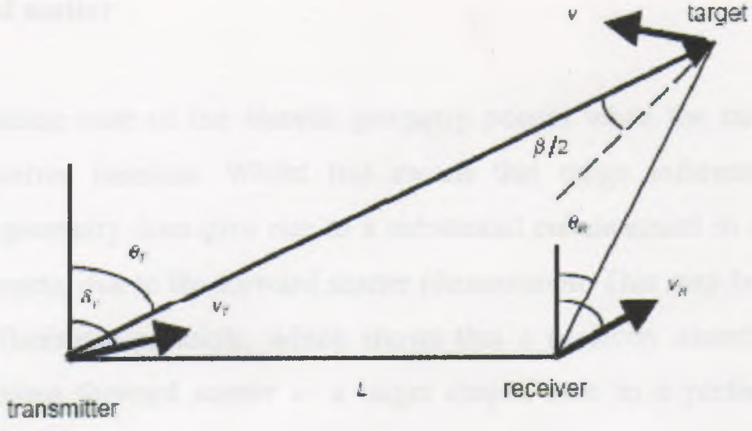

$$\beta = \theta_T - \theta_R$$

Figure 2.3 Bistatic Doppler (after Jackson (17)).

In the case when only the target is moving the Doppler shift is
given by:

$$f_D = \left(\frac{2V}{\lambda}\right)\cos\delta\cos\left(\beta/2\right) \tag{2.3}$$

2.2.2 Bistatic Radar Cross Section

The biostatic RCS of targets has been studied extensively [7], though relatively little has been published in the open literature. Early work [4, 18] resulted in the bistatic equivalence theorem, which states that the bistatic RCS b s is equal to the monostatic RCS at the bisector of the bistatic angle b, reduced in frequency by the factor cos (b/2), given (i) sufficiently smooth targets, (ii) no shadowing, and (iii) persistence of retro reflectors. These assumptions are unlikely to be universally valid, particularly for stealthy targets, so the results should be used with care.

2.2.3 Forward scatter

A limiting case of the bistatic geometry occurs when the target lies on the transmitter-receiver baseline. Whilst this means that range information cannot be obtained, the geometry does give rise to a substantial enhancement in scattering, even for stealthy targets, due to the forward scatter phenomenon. This may be understood by reference to Babinet's principle, which shows that a perfectly absorbing target will generate the same forward scatter as a target shaped hole in a perfectly conducting screen. The forward scatter RCS is approximately $\sigma_b = 4\pi A^2 / \lambda^2$ where A is the target projected area, and the angular width θ_B of the scattering will be of the order of λ / d radians, where d is the target linear dimension. Figure 3.3 shows how these vary with frequency, for a target of the size of a typical aircraft, and shows that frequencies around VHF / UHF are likely to be optimum for exploiting forward scatter.

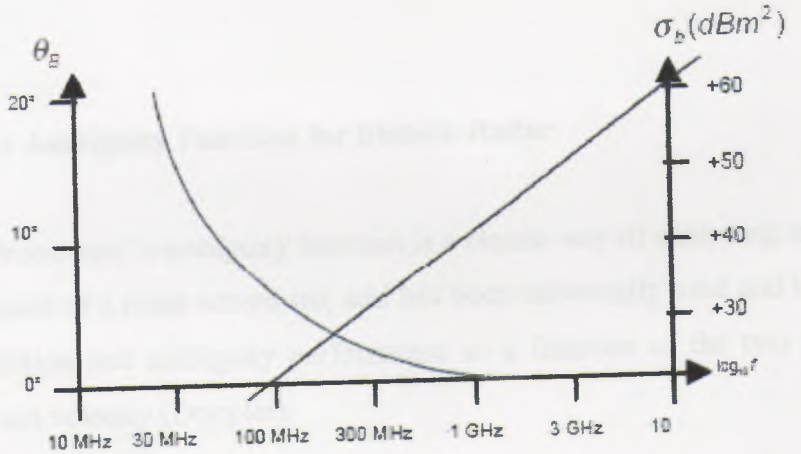

Figure 2.4 Variation of forward scatter RCS and angular width Of response (d= 10 m , A= 10 m^2)

2.2.4 Bistatic Clutter

Bistatic clutter is subject to greater variability than the monostatic case, because there are more variables associated with the geometry [31]. The clutter RCS σ_c is the product of the bistatic backscatter coefficient σ_b and the clutter resolution cell area A_c both σ_b and A_c are geometry dependent, with the maximum value of σ_b occurring at secular angles. There is relatively little experimental data available, and little work has been done in developing models for bistatic clutter.

There is some reason to suppose that bistatic sea clutter may be less 'spiky' than equivalent monostatic sea clutter, and hence that bistatic geometries may be more favorable for detection of small targets – but this remains to be investigated. There is thus much scope for new work on bistatic clutter; to gather data, to analyze the results, and to develop bistatic clutter models.

2.2.5 The Ambiguity Function for Bistatic Radar

Woodward's ambiguity function is a classic way of analyzing and presenting the performance of a radar waveform, and has been universally used and taught, presenting the resolution and ambiguity performance as a function of the two parameters delay (range) and velocity (Doppler).

$$|x(\tau,v)|^2 = \left|\int u(x)u^*(x+\tau)\exp(-j2\pi vx)\,dx\right|^2 \qquad (2.4)$$

With a bistatic or multistatic radar the situation is more complicated. Tsaoet.al. [29] have looked at this, and shown that the relationship between Doppler shift and target velocity, and between delay and range, are highly non-linear, and hence that the shape of the ambiguity functions is a strong function of geometry as well as waveform properties. They propose that the ambiguity function for bistatic radar should instead be written:

$$\left| x(R_{R_S}, R_{R_a}, V_H, V_a, \theta_R, L) \right|^2$$

$$\left| \int_{-\infty}^{\infty} \tilde{f}(t-\tau_a(R_{R_S},\theta_R,L))\, \tilde{f}^*(t-\tau_H(R_{R_S},\theta_R,L)) \exp\left[-j(\omega_{D_H}(R_{R_S},V_H,\theta_R,L)-\omega_{D_a}(R_{R_a},V_a,\theta_R,L))t\right] dt \right|^2 \tag{2.5}$$

We can take this further, and attempt to calculate and plot the ambiguity functions for bistatic and multistatic radars, although there does not seem to be the same elegant way of plotting the function as is the case with monostatic radars.

2.3 Applications of Multistatic Radar

2.3.1 Basaltic Radar on Mars Express

In bistatic radar experiments, the transmitter and receiver are spatially separated. When the transmitter orbits a distant planet, its antenna can direct relatively small amounts of power toward the remote surface, probing both its physical structure (roughness) and electrical properties (dielectric constant). Several bistatic radar experiments are planned as part of Mars Express Radio Science (MARS) investigations. Stations on Earth will receive the surface echoes at both 3.6 and 13.1 cm wavelengths. Similar experiments have been conducted previously using Viking and Mars Global Surveyor spacecraft.

In quasi-specular experiments, the spacecraft antenna is aimed toward the point on the mean planetary surface which would give mirror-like (specular) reflection toward Earth. Because the path length via the specular point changes at a different rate than the direct-to-Earth path, the surface echo may be distinguished at the receiver by its Doppler shift. When the surface is rough, many reflections contribute to the total echo, each with a slightly different Doppler; dispersion of the composite echo is proportional to the *rms* roughness of the surface in the vicinity of the specular point.

To first order, the reflected power in the echo is proportional to the Fresnel reflection coefficient of the dielectric material making up the top few centimeters of surface. Volcanic plains and the "Stealth" region west of Tharsis Montes will be studied using Mars Express bistatic radar.

Icy surfaces sometimes display anomalously high radar backscatter; Europe, Ganymede, and Callisto are distinctive in this way. The south residual polar cap on Mars is also radar bright; but the north appears not – or, at least, less so. Bistatic radar experiments conducted in either a backscatter geometry (as the spacecraft antenna sweeps across the surface in the anti-Earth direction) or in spotlight mode (where the antenna's bore sight is fixed on a single surface point, which also passes through the backscatter condition) may be helpful in understanding the nature of icy surfaces on Mars.

CHAPTER THREE

EXAMPLES OF PASSIVE COHERENT SYSTEM

3.1 Passive Coherent Location

The use of broadcast or communications signals as 'illuminators of opportunity' has become known as 'passive coherent location' (PCL) or 'hitchhiking', and there has been particular interest in this aspect of bistatic radar in recent years.

The properties of transmissions for these purposes can be assessed in terms of (i) power density at the target, (ii) spatial and temporal coverage, and (iii) waveform. The power density $\Phi(in\, W/m^2)$ at the target is evaluated from:

$$\Phi = \frac{P_t G_t}{4\pi r^2} \tag{3.1}$$

The spatial and temporal coverage will depend on the location of the transmitter, its radiation pattern, and (for example) whether it is stationary or moving and whether it operates for 24 hours per day or not. In some cases the vertical plane radiation pattern of TV or radio transmissions is deliberately shaped so as to avoid wasting power above the horizontal. The coverage achieved by VHF FM radio and TV transmissions is substantial. This is because such systems have to be designed to cope with non line-of-sight propagation and very inefficient antenna and receiver systems. Cell phone base stations are also potentially useful as PCL illuminators [34, 36]; whilst these are of rather lower power, there are many of them, especially in urban areas. Satellite-borne illuminators, such as DBS TV [12], satellite communications and navigation [2, 19] and space borne radar [13, 23, 35] are also of interest.

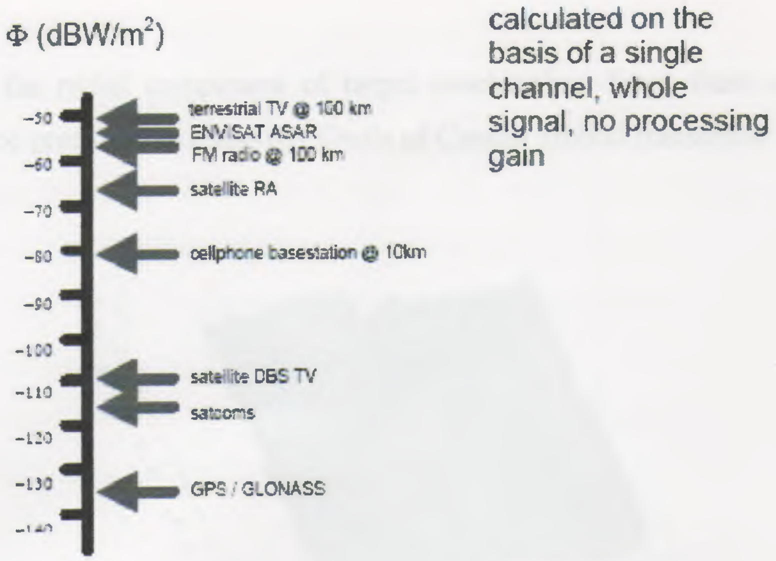

Fig 3.1 Power density Φ for various PCL illuminators.

The waveform parameters of interest are the frequency, bandwidth, ambiguity function, and stability. In some cases it may be appropriate only to use a portion of the available signal (for example, to avoid ambiguities associated with the line and frame repetition rate of analogue TV modulation). In such cases the transmit power value used in equation (3.4) should be appropriate.

Figure 3.1 shows the values of for various PCL illuminators, under various assumptions. These are calculated on the basis of a single channel, the whole signal bandwidth, and no processing gain.

The detection performance can then be estimated from:

$$(r_2)_{\max} = \left(\frac{\Phi \sigma_b \lambda^2 G_p}{(4\pi)^2 (S/N)_{\min}\, kT_0 BF} \right)^{1/2} \tag{3.2}$$

Where G_p is the processing gain, which is the product of the waveform bandwidth and the integration dwell time. The integration dwell time in turn depends on the waveform coherence and the target dynamics. As a rule of thumb, the maximum integration dwell time is given by:

$$T_{\max} = \left(\frac{\lambda}{A_R} \right)^{1/2} , \tag{3.3}$$

where AR is the radial component of target acceleration. From these equations the coverage can be predicted in terms of Ovals of Cassini around transmitter and receiver.

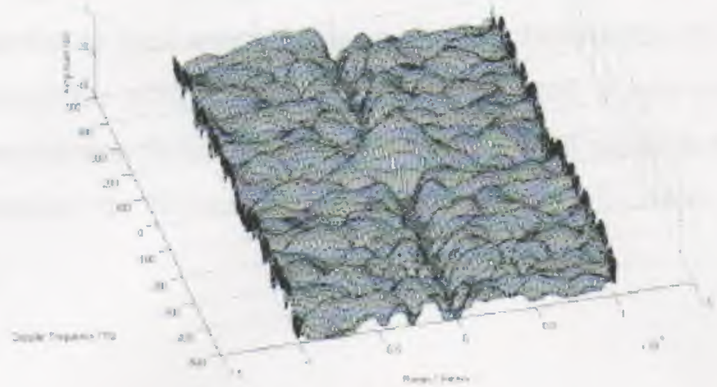

(a)

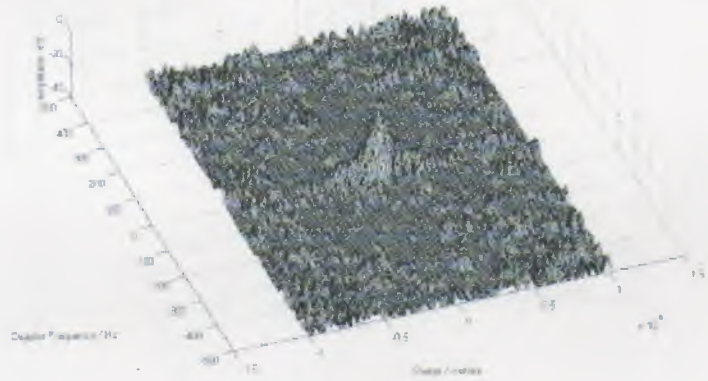

(b)

Figure 3.2. Typical ambiguity functions: (a) BBC Radio 4 transmission (93.5 MHz) and (b) digital audio broadcast transmission (222.4 MHz).

The waveform properties of a variety of PCL illuminators (VHF FM radio, analogue and digital TV, digital audio broadcast (DAB) and GSM at 900 and 1800 MHz) have been assessed by digitizing off-air waveforms and calculating and plotting their ambiguity functions [14]. The receiving system was based on a HP8565A spectrum analyzer, digitizing the 21.4 MHz IF output by means of an Echotek ECDR-214-PCI Digitizer card mounted in a PC. The system has the advantage of great flexibility, since the centre frequency and bandwidth of the receiver can be set by the controls of the spectrum analyzer. The rather high noise figure of the spectrum analyzer is not a disadvantage, since all of the signals are of high power and propagation is line-of-sight. Figure 6 shows typical ambiguity functions derived using this system of (a) BBC Radio 4 at 93.5 MHz, for which the program content is speech (an announcer reading the news), and (b) a digital audio broadcast (DAB) signal at 222.4 MHz. Both show range resolution appropriate to their instantaneous modulation bandwidths (9.1 and 78.6 kHz respectively), though the difference in the sidelobe structure is very evident, showing that the digital modulation format is far superior because the signal is more noise-like. Table 3.1 summarizes the measured ambiguity function Performance of the various signals captured.

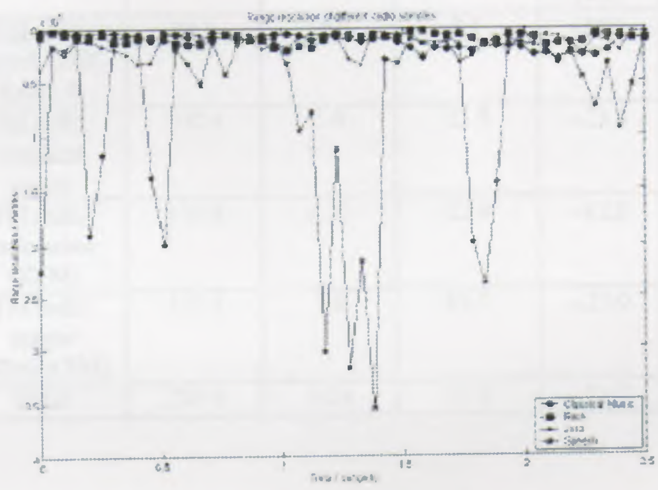

Fig 3.3.Variation in range resolution against time for four types of VHF FM radio modulation.

It is also important to know how these properties vary with time, as variations in the form of the ambiguity function will determine the radio system performance. Fig. 3.3 shows variation in range resolution of four VHF FM radio transmissions, calculated from the −3 dB width of the zero Doppler cut through the ambiguity function, over a 2.5 second interval.

It is evident that for the three types of music the range resolution varies by a factor of two or three, but for the speech modulation the range resolution is badly degraded during pauses between words, by a factor of ten or more.

Furthermore, when we also take into account the dependence of the ambiguity function on geometry (equation 5), it can be seen that there is scope for adaptively choosing the signals from a variety of transmitters in a multistatic PCL system, selecting those for which the geometry and instantaneous modulation are favorable.

Table 3.1 Properties of Ambiguity Function of Various Types of Broadcast and Communications Signal

signal	frequency (MHz)	range resolution (km)	effective bandwidth (kHz)	peak range sidelobe level (dB)	peak Doppler sidelobe level (dB)
FM radio: speech (BBC Radio 4)	93.5	16.5	9.1	−19.1	−46.5
FM radio: classical music	100.6	5.8	25.9	−23.9	−32.5
FM radio: rock music (XFM)	104.9	6.55	22.9	−12.0	−26.0
FM radio: reggae (Choice FM)	107.1	1.8	83.5	−27.0	−39.5
DAB	219.4	1.54	97.1	−11.7	−38.0
Analogue TV: chrominance sub-carrier	491.55	9.61	15.6	−0.2	−9.1
Digital TV (DVB-T)	505.0	1.72	87.1	−18.5	−34.6
GSM 900	944.6	1.8	83.3	−9.3	−46.7
GSM 1800	1833.6	2.62	57.2	−6.9	−43.8

3.2 Examples of System

3.2.1 Amateur Radio Forward Scatter Experiment

An interesting early example of PCL was given by a radio amateur, the Rev. Dr P.W. Sollom, who had noticed a fluttering effect on VHF amateur signals due to the interference between direct signals and Doppler-shifted echoes from aircraft [24]. The same effect may easily be observed with VHF FM radio and VHF or UHF TV, and works best when the direct signal and scattered signal are of comparable amplitude. He devised an elegant set of experiments using a VHF TV signal located in northern France as illuminator, and built a two-Yagi interferometer, such that a moving target would pass through the interferometer grating lobes, allowing the target motion to be estimated from the amplitude modulation.

3.2.2 Non-co-operative Radar Illuminators

The first work on bistatic radar at University College London was undertaken in the late 1970s. Schoenenberger and Forrest designed and built a system using a UHF Air Traffic Control radar at Heathrow airport as illuminator, and investigated particularly the problems of synchronization between receiver and transmitter [28]. Figure 8 shows a typical PPI display from this system. A real-time co-ordinate correction scheme was also developed for this system.

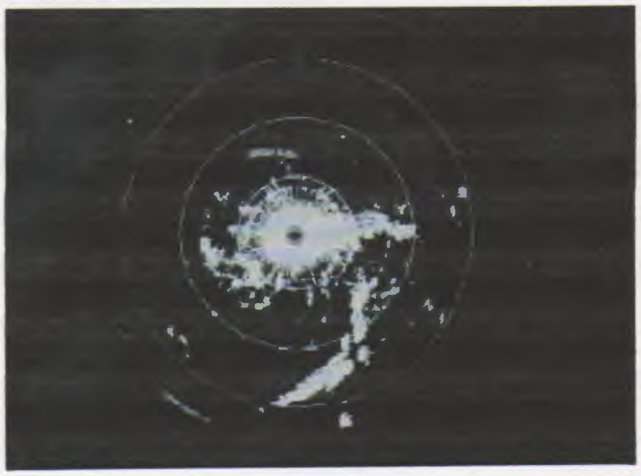

Fig.3.4PPI display from UCL bistatic radar system.

Further developments included a digital beamforming array [9] for pulse chasing experiments (Fig. 3.4) and a coherent MTI system using clutter from stable local echoes as a phase reference [10].

Fig.3.5Digital beamforming array used for pulse chasing experiments with UCL bistatic radar system.

3.2.3 Television-based Biostatic Radar

Subsequent work at UCL attempted to use UHF television transmissions as illuminators of opportunity, to detect aircraft targets landing and taking off from Heathrow airport, to the west of London [11]. Figure 3.5 shows the geometry. The results showed that although the television waveforms are very suitable in terms of power and coverage, the analogue television modulation format suffers from ambiguities at the 64 μs line repetition rate, which correspond to a bistatic range of 9.6 km.

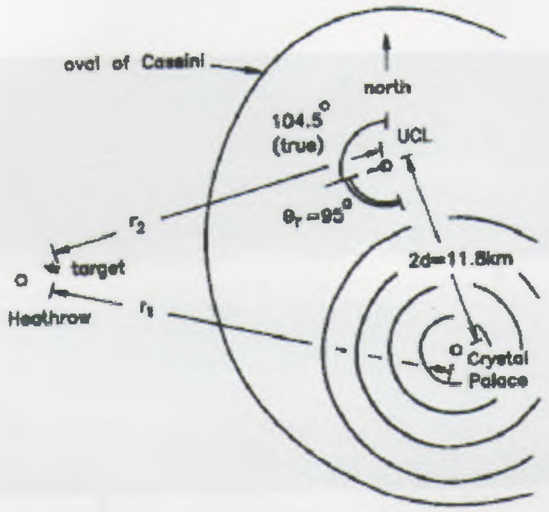

Figure 3.6. Horizontal-plane geometry of crystal place television transmitter and Heathrow.

3.2.4 TV-based Forward Scatter System

Howland [16] developed a UHF forward scatter system based on television transmissions. Because a forward scatter system is not able to provide range information, he adopted a different approach, measuring angle of arrival (from a two-element interferometer) and Doppler shift of the vision carrier of the television signal. Target tracking was done by an extended Kalman filter algorithm.

He was able to demonstrate tracking of aircraft targets at ranges well in excess of 100 km (Fig. 3.7).

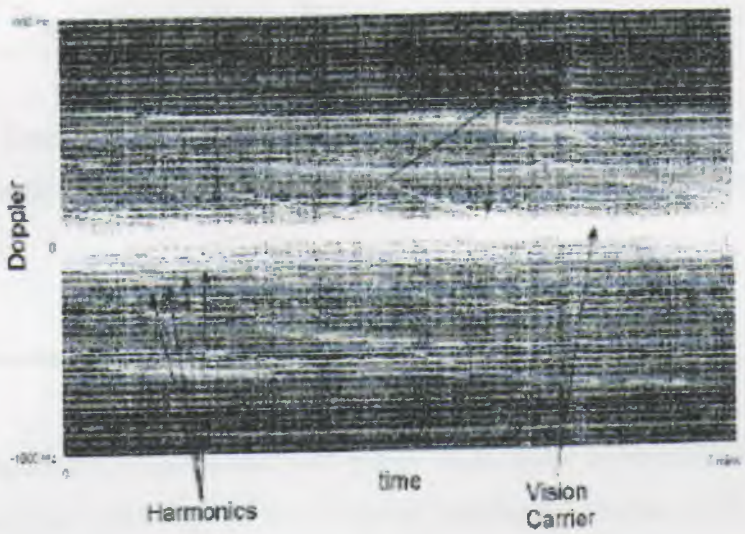

Fig. 3.7 Example power spectrum against time, around TV vision carrier (after Howland [16].

He was able to demonstrate tracking of aircraft targets at ranges well in excess of 100 km

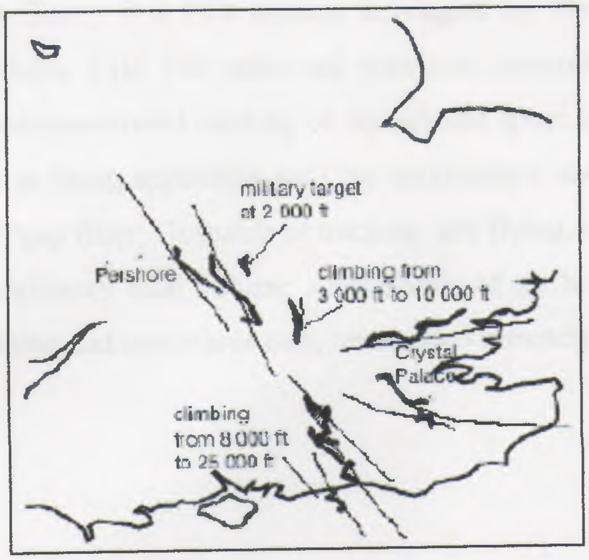

Figure .3.8. Track estimates formed on 21 February 1997 between 14:00 and 14:07, compared with secondary radar tracks for the same aircraft (after Howland [16]).

3.2.5 The Manastash Ridge Radar

The Manastash Ridge Radar is a rather remarkable system conceived and built by John Sahr of the University of Washington, Seattle, for studies of the ionosphere. It uses a single VHF radio transmitter as illuminator, and a receiver separated from the transmitter by a large mountain range (Mt. Rainier). The receiving system is based on a standard digitizer card and PC, and is extremely simple and cheap (~ $15k). Synchronization is achieved by GPS, giving uncertainties of 100 ns in timing (= 15 m in range) and 0.01 Hz in Doppler (= 1 cm/s in velocity). The system provides quasi-real-time imagery, out to ranges in excess of 1,000 km, on their website [36]. Although the purpose of the system is for ionospheric studies, it also routinely detects aircraft targets at ranges up to ~ 100 km.

Such a system demonstrates vividly that high performance can be achieved from simple and inexpensive PCL systems.

3.2.6 Silent Sentry

Silent Sentry is a PCL system developed by the Lockheed Martin company, based on multiple VHF FM radio and television transmissions. In its present version (SSIII) it has demonstrated tracking of aircraft and space targets at impressive ranges. It is advertised as being applicable to: air surveillance and tracking in areas of limited coverage – a 'gap filler; capable of tracking low flying, non-cooperative, slow moving targets; continuous total volume surveillance of air breathing and ballistic objects; low acquisition and operations cost, unattended remotely managed.

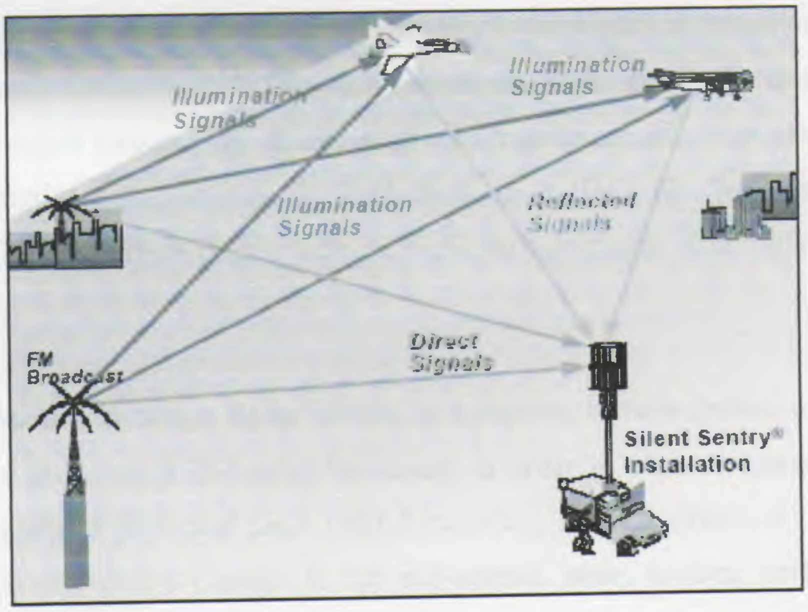

Figure 3.9. Principles of Operation of Client Sentry (figure courtesy of Lockheed Martin)

CHAPTER FOUR

PASSIVE COHERENT SCATTER RADAR INTERFEROMETER IMPLEMENTAION, OBSERVATIONS, AND ANALYSIS

4.1 Introduction

In coherent scatter studies of the ionosphere, interferometric techniques have frequently been used to estimate the transverse structure and position of scattering regions within the field of view [Farley et al., 1981; Providakes et al., 1983]. Recently, passive coherent radar techniques have been applied in studies of the ionosphere; Sahr and Lind [1997] describe a VHF passive radar for observation of the high latitude E-region which provides Doppler power spectrum as a function of range, with high range, time, and Doppler resolution. Howland [1999] has implemented an interferometer using the passive radar technique with television broadcasts and successfully used it to track compact aerospace targets. We describe here an interferometric extension of range-Doppler estimation using commercial FM broadcasts at 100 MHz. We present the first observations of ionospheric targets with such an instrument, and offer initial analysis of these data.

The Manastash Ridge Radar (MRR) is a passive, bistatic system which detects the scatter of commercial FM radio broadcasts in order to observe ionospheric _eld-aligned irregularities [Sahr and Lind, 1997; Lind et al., 1999]. Its field of view covers a region over southwestern Canada in the sub-auroral zone, looking northward from central Washington State. The MRR provides range and Doppler information at VHF frequencies (near 100 MHz) with superb sensitivity and resolution that is comparable or superior to that of conventional coherent radars. The addition of interferometry permits the estimation of transverse structure as well, extending the data sets it provides into ones which are functionally equivalent to those of conventional active radar interferometers [Providakes et al., 1985], and allowing direct comparison between these data sets.

The simplicity, safety, and low cost of passive radar permits continuous and unattended operation; a separate report [Meyer et al., 2004] will summarize several thousand irregularity events observed during the nearly continuous operation of the MRR since January 2002. 1.1 The Manastash Ridge Radar Commercial FM radio broadcasts provide convenient and surprisingly useful illumination for radio scattering studies of the ionosphere. FM transmitters are CW, broadcast antennas are usually omnidirectional, and the effective radiated power is high (typically 100 kW). The 100 MHz carrier frequency is nearly immune to ionospheric refraction and atmospheric absorption effects, yet scatters readily from meter-scale plasma turbulence. Most importantly, the typical FM waveform has an excellent ambiguity function in the average sense [Hansen, 1994], often completely free of range and Doppler aliasing. In essence, the FM transmission acts like a stochastically coded long pulse [Harmon, 2002], which is very useful for overspread targets such as Bragg scattering ion-acoustic turbulence in the ionosphere. The bandwidth of the FM transmission is large compared to that of actuations in the ionospheric plasma, and this permits overspread target pulse compression. A report on efficient evaluation of the detection algorithm is in preparation [Morabito et al., 2004]. To recover the time series of the scatterer, we must correlate the scattered signal with the original illuminating signal. Rather than attempt to distinguish the direct-path and scattered signals in a single receiver, we use separate receivers: one near the transmitter to provide a reference, and another located approximately 150 km away, behind the Cascade mountain range, so that it is primarily exposed only to the scattered signal. This drastically reduces

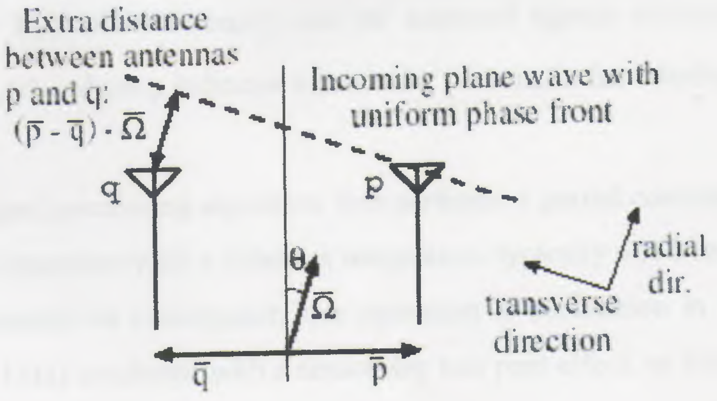

Figure 4.1. An illustration of radar interferometry and our notation.

The vectors $\bar{P}$ and $\bar{q}$ carry antenna baseline information; the unit vector $\tilde{\Omega}$ carries the angle of arrival (θ) information. The interferometer phase is related to all three vectors, as well as the wave number of the original illuminating waveform. The dynamic range required of the receivers. We have implemented the interferometer with multiple antennas collecting the scattered signal, arranged in such a way as to emphasize azimuthal structure; each antenna's signal is correlated with the same reference signal. A sketch of the interferometer geometry is shown in Figure 4.1. Currently there are three antennas in the system which collect scatter, providing possible baselines of 3.5λ, 12.5λ, and 16λ (≈ 47m). The observations reported here have been performed with the 16λ separation; thus, 32 separate interferometer lobes are contained in the full 180° field of view. The shorter baselines were recently constructed to address the azimuthal aliasing some of the azimuthal ambiguity may be removed by considering the gain patterns of the receiving antennas, but we do not address this here. The strongly field-aligned nature of E region irregularities further constrains possible target location, however, and in many cases we are able to resolve even the potentially wide auroral targets coherently.

4.2 Implementation

To extract the interferometric information, we pursue the suggestion for interferometry made by Sahr and Lind [1997]. We denote the signal arising from the transmitter by $x(t)$ (the reference), and the scattered signals collected by the remote receivers by $y_p(t)$, where p indicates a particular antenna in the interferometric array.

Our signal processing algorithm first performs a partial correlation (essentially a matched filter operation with a coherent integration, typically of 50 samples or greater). When implemented on a computer, this operation is decimation in the raw data rate (typically 100 kHz) combined with a smoothing low pass effect, as follows:

$$z_p(r_0,t)= \sum_{v=0}^{D-1\geq 49} y_p(t+t')x^*(t+t'-r_0) \tag{4.1}$$

Where t advances in multiples of the decimation factor D. The resulting signal $z_p(r_0,t)$ is a time series of the scatterer at a particular bistatic range $r \approx r_0 \times c/2$ which evolves at the low bandwidth rate of the scatterer (about 2 kHz).

Because of the coherent integration, the clutter from signals arriving from other ranges is greatly reduced and spectrally whitened; thus $z_p(r_0,t)$ is an unbiased estimate of the scattering voltage. Sequences of $z_p(r_0,t)$ may be assembled into time series for conventional FFT-based spectrum estimation:

$$z_p(r_0,f) = FFT\left|z_p(r_0,t)\right| \tag{4.2}$$

$$P_{pp}(r_0,f) = \frac{1}{M}\sum_M\left|Z_p(r_0,f)\right|^2 \tag{4.3}$$

Where $P_{pp}(r_0,f)$ is the power spectrum received on antenna p. The number of incoherent averages M depends on the duration of the observation and the number of points used in each FFT. In Figure 2 we provide an example of 256-point Doppler power spectra as a function of range, estimated from 10 seconds of raw data, using an incoherent average of 78 spectra.

The decimated, unbiased time series is also available for conventional cross spectral analysis [Farley et al., 1981]. We correlate voltage spectra from different antennas in the frequency domain as follows:

$$P_{pp}(r_0,f)=\frac{1}{L}\sum_L Z_p(r_0,f)Z_q^*(r_0,f) \tag{4.4}$$

Here the sum over L represents point-by-point incoherent averaging of L cross-power spectra. Normalizing the cross spectrum by the self power on each antenna, we have

$$C_{pq}(r_0,f)=\frac{P_{pq}(r_0,f)}{\sqrt{P_{pp}(r_0,f)P_{qq}(r_0,f)}} \tag{4.5}$$

The normalized cross spectrum $C_{pq}(r_0,f)$ is a complex-valued function which represents the coherence and phase shift between the signals arriving at antennas p and q for each range delay r0 and for each Doppler shift f.

The phase of the cross spectrum ϕ is directly related to the angle of arrival of the signal incident on the antennas, denoted θ: however, the potential to uniquely determine θ: depends on the spacing between the antennas with respect to the wavelength of the incoming signal. An antenna spacing of $\frac{\lambda}{2}$ 2 allows a full 180° of azimuth to be mapped uniquely onto the available 2π radians in. ϕ Where the coherence is high, we expect the interferometer phase ϕ to be compact and organized, since the majority of the power is coming from a single direction. Also, because the noise processes polluting the two antennas are uncorrelated, the expected noise floor of Ppq(r0; f) is zero for ranges and Dopplers in which no echo is present. It will be necessary, however, to compensate for self-clutter and other interfering signals which are correlated on the interferometer antennas, as we show below.

4.2.1 The Interferometer Cross-Correlation Estimator

To illustrate the properties of our interferometer, we describe an estimator for cross correlation (the Fourier transform of the cross spectrum) for passive radar. With a conventional

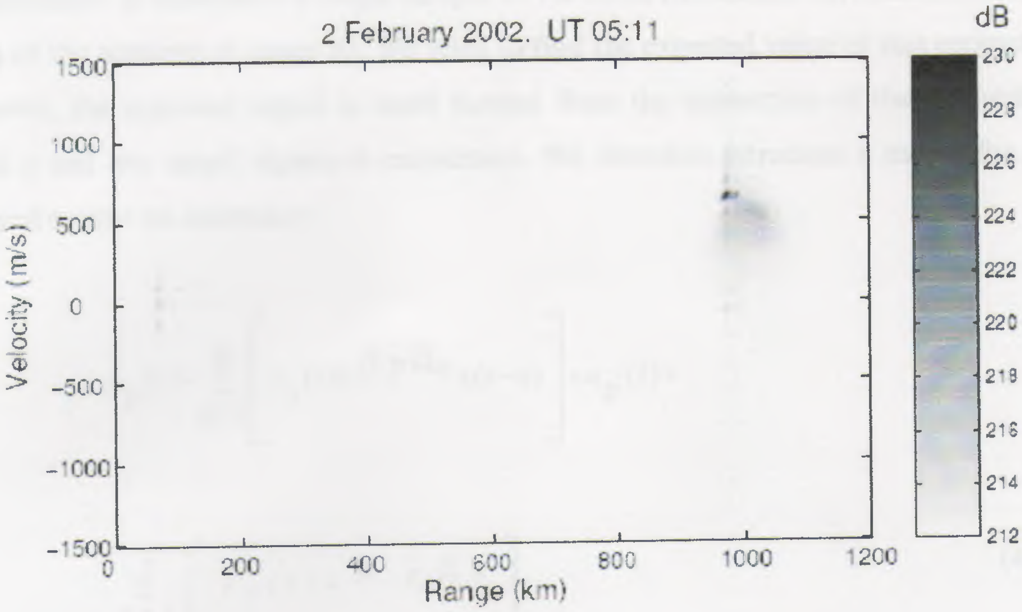

Figure4.2. A range-Doppler diagram, the typical data product of MRR. Reflections from the Cascade mountain range can be seen at zero Doppler near 100 km; note the prominent (but low) ambiguity sidelobes of the FM broadcast. At a range of 1000 km, an echo due to ionospheric plasma turbulence is present. (Pulsed) radar, the natural estimator for the complex cross correlation of a target signal on two antennas p and q takes the form

$$v_p(t)v_q^*(t-T) \tag{4.6}$$

Where v_p and v_q are voltages on the scatterreceiving antennas. However, in the passive radar case, we first need to deconvolve the reference signal from the received scatter, as shown above. The additional $z=yx^*$ correlation step results in a much larger number of terms to consider when evaluating the statistics of the passive radar interferometer estimator (denoted K):

$$\hat{K}=z_p(r_0,t)z_q^*(r_0,t-T) \quad (4.7)$$

$$=y_p(t)x^*(t-r_0)y_q^*(t-T)x(t-r_0-T) \tag{4.8}$$

The estimate ^K represents a single sample of the cross correlation between antennas p and q of the scatterer at range r0. We wish to find the expected value of this estimator. However, the scattered signal is itself formed from the interaction of the transmitter signal x and any target signals it encounters. We therefore introduce a model for the received scatter on antenna p:

$$y_p(t) = \sum_{n=1}^{R} \left[s_n(t) e^{jk\bar{p}\bar{\Omega}_n} x(t-n) \right] + n_p(t) +$$

$$\sum_{i=1}^{I} \left[\gamma_i(t) e^{jk\bar{p}\bar{\Omega}_i} \right] \tag{4.9}$$

Here R is the number of contributing ranges, equal to approximately 800, or 1200 km in the usual implementation of MRR; after this distance, E-region targets fall below the horizon.

We must include all R ranges, because the transmitter operates continuously. The complex signals $s_n(t)$ (assumed to be Gaussian distributed) contain amplitude and Doppler information about the targets at each range; k is the wave number of the transmitter signal. We have written the phase term due to the angle of arrival as a dot product between vectors $\bar{\Omega}$ is a unit vector in the direction of the target with respect to the origin (defined as the midpoint between the two antennas), and $\bar{p}$ represents the location of antenna p (and therefore carries information about the distance between that antenna and the origin). These vectors can be seen in the interferometry illustration of Figure 1. For simplicity in this model, we assume the scattering signals are point targets in azimuth. Also present are a sum over all interference sources γ_i and a receiver noise term, np, which is specified to antenna p. By specifies, we mean that the receiver noise associated with the signal from one antenna is uncorrelated with that associated with other antennas Substituting this model into the K estimator above yields second- and fourth-order correlations in the transmitted signal, target signals and interfering signals, as follows (we have dropped complex conjugates and time arguments in favor of compact notation):

$$\left\langle \hat{K} \right\rangle = \sum_{i=1}^{I} \sum_{j=1}^{I} \delta_{ij} \left\langle \gamma_i \gamma_j \right\rangle \left\langle xx \right\rangle \left\langle e^{jk(\bar{p}\bar{\Omega}_t - \bar{q}\bar{\Omega}_j)} \right\rangle +$$

$$\sum_{n-1}^{R} \sum_{m-1}^{R} \delta_{nm} \left\langle s_n s_m \right\rangle \left\langle e^{jk(\bar{p}\bar{\Omega}_n - \bar{q}\bar{\Omega}_m} \right\rangle \times \left\langle xxx \right\rangle \quad (4.10)$$

We have assumed that the transmitter signal, target signals, interference sources, and receiver noise are all zero mean and independent of each other. We likewise assume that target signals at different ranges are uncorrelated (thus the Kronecker δ_{nm}), and that different sources of interference are uncorrelated (δ_{ij}). Next, proceeding in the manner of Sahr and Lind [1997] and Meyer [2003], we denote correlation functions by R() and use the Isserlis Gaussian moment theorem [Isserlis, 1918] to simplify the fourth-order correlation $\langle xxxx \rangle$:

$$\left\langle \hat{K} \right\rangle = \sum_{i=1}^{I} R_{\gamma,i}(T) R_x^*(T) \left\langle e^{jk(\bar{p}-\bar{q})\bar{\Omega}_t} \right\rangle +$$

$$\sum_{n=1}^{R} R_{s,n}(T) \left\langle e^{jk(\bar{p}-\bar{q})\bar{\Omega}_n} \right\rangle \times \quad (4.11)$$

$$\left[\langle xx \rangle \langle xx \rangle + \langle xx \rangle \langle xx \rangle \right]$$

Finally, we use the approximation

$$R_x(T) = R_x(0)\delta(T)$$

This is justified when the sampling period for x (t) is greater than its correlation time such that x (t) is a white process, a reasonable claim in this case. We arrive at

$$\left\langle \hat{K} \right\rangle = R_x^2(0)\left\langle e^{jk(\bar{p}-\bar{q})\bar{\Omega}_{r0}} \right\rangle R_{s,r0}(T) +$$

$$\delta(T)\left[R_x^2(0)\right]\sum_{n=1}^{R}\left\langle e^{jk(\bar{p}-\bar{q})\bar{\Omega}_n} \right\rangle R_{s,n}(0) + \tag{4.12}$$

$$R_x(0)\sum_{i=1}^{I}\left\langle e^{jk(\bar{p}-\bar{q})\bar{\Omega}_t} \right\rangle R_{\gamma,i}(0)$$

which is the expected value of the interferometer cross correlation estimator for a target at range r0. This expression contains the autocorrelation of the target that we seek, $R_{s,r_0}(\tau)$, as well as the interferometer phase term $k(\bar{p}-\bar{q})\cdot\bar{\Omega}_{r_0}$, which is related to the angle of arrival of the target signal. The transmitter power $R_x(0)$ is also present in each term. However, the estimate is biased by \self-clutter" and all sources of interference arriving on the scatter receiving antennas. The self-clutter bias is similar to the excess power in the zero lag of all autocorrelation function estimates of overspread targets [Farley, 1969]. As indicated by the $\delta(\tau)$ term discussed earlier, the self-clutter and the bias due to interference are present only at lags shorter than the correlation time of the transmitter signal. Therefore, this \white bias" will translate into a flat noise floor in the frequency domain, degrading signal delectability, and also affecting the phase spectrum. At present we estimate and remove the interferometer bias by computing the cross spectrum at a distant range which is presumed to be free of any detectable scatter. We then subtract this bias estimate from the cross spectrum at the range of interest. Point-by-point subtraction allows us to distinguish between the bias that may be present in different Doppler bins, which will be useful in a frequency-selective fading environment, or in the presence of narrowband interference sources. Finally, we note that the cross correlation esti-

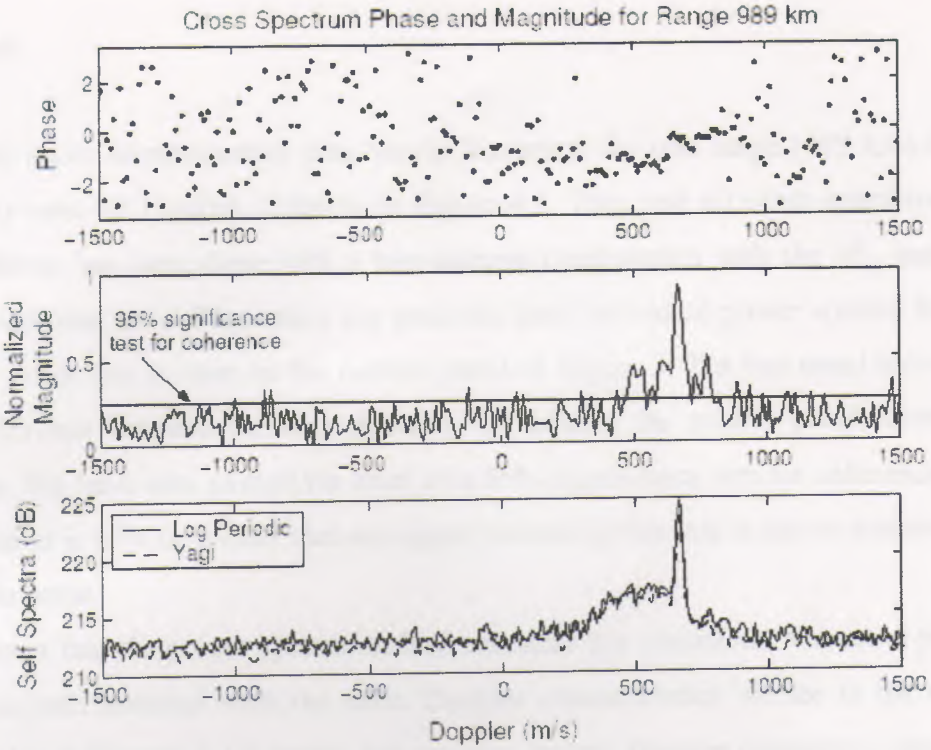

Figure 4.3. The cross spectrum and self spectra for one range

In the 2 February 2002 echo from Figure 4.2. Due to the highly organized phase in the same area with significant coherence levels, we observe that the echo seems limited to one interferometer lobe. The phase width implies a scattering volume of approximately 15 km. mator discussed above has the desirable secondmoment property of consistency, by extension of the single-antenna case worked out by Sahr and Lind [1997].

4.3 Results

We show interferometer data versus frequency for one range (989 km) in the irregularity echo of Figure4. 2 below in Figure 4.3. This, and all other interferometer data we show, has been done with a two-antenna combination with the 16_ baseline. The two antennas are a Yagi and a log periodic; their individual power spectra for this particular event can be seen in the bottom panel of Figure 3. The top panel shows the phase difference between the two antennas, in radians; the middle panel shows the coherence. We have also plotted the level of a 95% significance test for coherence; i.e., the likelihood is 95% or greater that any signal exceeding this line is due to scattering as opposed to noise.

It is apparent that the power spectra on both antennas are consistent; a spectral peak is present on both antennas with the same Doppler characteristics we see in the range-Doppler plot of Figure4.2. (A bright, fast moving, narrow Doppler component alongside a slower moving type 2 body). As with conventional interferometry, the cross spectrum phase and coherence are also consistent with coherent backscatter in that the coherence becomes large in the same area that the phase becomes organized. We therefore conclude that this auroral echo is most likely contained within one interferometer lobe (approximately 100 km wide at this range).

In principle, it is possible to estimate the angular width of the target from the coherence [Farley et al., 1981]; however, it is also possible to

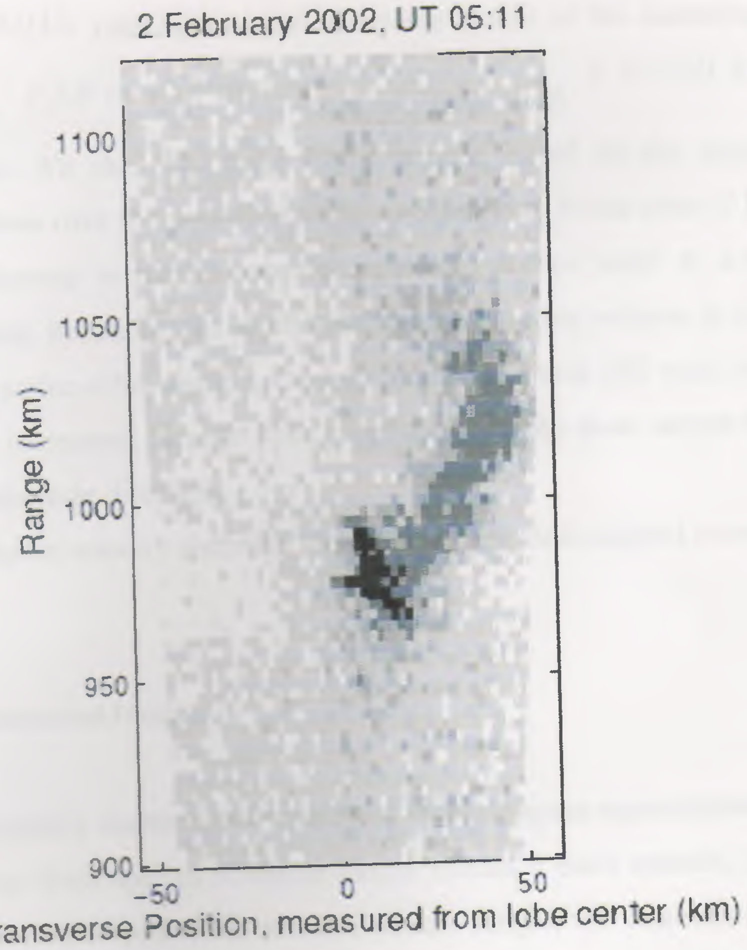

Figure 4.4 The 2 February 2002 auroral echo, represented in a 2-D phase distribution image of range vs. transverse width .

to interpret the range of the phase estimates in those Doppler bins where the phase is concentrated (and where the coherence is significant) as a measure of the transverse width of the scattering volume. In this case, the range of the phase estimates (denoted $\Delta\phi$) over the area of significant coherence is about 1.5 radians (by inspection of the plot). We can approximate the azimuth extent, $\Delta\theta$, with $\Delta\phi/(kd)$, where d is the distance between the antennas, if we assume the target is nearly broadside to the interferometer axis (using $\phi = kd\sin\theta$ and $\sin\theta \approx \theta$ for small θ). Then, with the 16λ antenna baseline, $kd = 16\lambda \times 2\pi/\lambda \approx 100$; thus, the azimuth extent $\Delta\theta \approx 0.015$ radians, and the transverse extent of the scattering volume is approximated by $r\Delta\theta \approx 15$ km, where we have used $r \approx 989$ km from a-priori knowledge. We can also make interpretations based on the structure of the interferometer phase over the area of significant coherence. In the case of Figure 3, the phase estimates appear to remain roughly constant, but then \step" to a new level in faster Doppler bins, indicating the separation of the scattering volume in the transverse dimension. The entire echo spans a Doppler width of about 500 m/s; the change in phase over these increasing Doppler bins suggests a velocity shear across the scattering volume in the transverse direction.

In general, we expect velocity shears to accompany large field-aligned currents.

4.3.1 Two-Dimensional Images

The irregularity scattering volume from Figure 2 spans approximately 100 km in range. Examining cross spectra at nearer ranges reveals a more smooth, linear upward trend in phase across Doppler, but at more distant ranges, the discontinuity discussed above becomes more pronounced, indicating the complete separation of he slower- and faster-moving parts of the scatterer.

Finally, at far ranges where the strong, narrow Doppler feature does not exist, and only the broader type 2 echo remains, the interferometer phase stays roughly constant over the entire Doppler span of the echo, suggesting a single scattering volume. It is clear that much can be learned by examining interferometer data over the complete range span of an irregularity echo. Therefore, we also use a phase distribution method to create two-dimensional \images" of range versus transverse dimension, such as the one in Figure 4. Here we show a grid of intensities {total power received at each range (frequency information is integrated out) {separated, via interferometer information, into 50 phase bins. Essentially, we create phase histograms at each range, and weight them by the appropriate cross spectrum magnitude. Our transverse resolution in Figure 4 is approximately 2 km, while the range resolution is 1.5 km. The larger-scale structure of the echo is now easily visible: the strong, shorter echo appears to split from the lower-intensity type 2 echoes (which we know from Doppler information to be moving more slowly than the strong echo). This observation is consistent with the speculations from the individual cross spectra above. Since our interferometer baseline is quite large, Our data is strongly aliased in angle. Therefore, it is unclear whether these two echoes are part of the same scattering volume, or whether they exist in different parts of the sky. Also, the absolute location (of either or both echoes) in the sky is unknown. However, recognizing the highly field-aligned nature of these phenomena, it is reasonable to speculate that the observed scatter exists in a single region of the sky. Auroral E-region irregularities are generally confined to exist within 1 degree of perpendicular aspect angle. To achieve sufficient backscatter, then, a radar must observe with a line of sight that is nearly perpendicular to the terrestrial magnetic field, B. At a range of 1000 km, our radar field of view stays within 2° of perpendicular aspect angle over a transverse span of about 200 km. At this same range, our interferometer beams are approximately 100 km wide, indicating that any irregularity scatter we see will most likely be contained within two lobes of the interferometer. Figure 5 shows another example of a two-dimensional interferometer image (right panel) and its range-Doppler counterpart (left panel). This echo, observed on 24 March 2002, spans over 100 km in range and has similar interesting Doppler features to the example above. It appears to have a type 4 component (narrow spectral peak near 900 m/s), again accompanied by a weaker and slower-moving type 2 feature. Doppler characteristics such as these are often seen together [Schlegel, 1996]. The interferometer image suggests three distinct components within a limited scattering volume; this is not an apparent structure when only range and Doppler information are considered. Near the 1100 km mark, in ranges which contain both the type 2 and type 4 echoes, the image does not show a clear delineation between separate scattering volumes. To investigate this area, we examine interferometer phase spectra at individual ranges; several of these (1088{1104 km) are shown in Figure 6 along with corresponding single-antenna power spectra. We note that the interferometer phase remains approximately constant over both the type 2 and type 4 Doppler features. Although this evidence does not necessarily indicate that the different Doppler features exist in the same location (due to aliasing), it is nevertheless strongly suggestive, especially in light of the aspect angle dependency discussed above.

4.3.2 Velocity and Electric Field

Measurements

It is also possible to estimate the transverse drift velocity of a scatterer by observing the temporal progression of interferometer phase information. This apparent motion can arise in two ways. First, a stable large scale electric field structure can convict across the field of view in an orderly fashion. Second, a time varying electric field can sporadically excite irregularities in adjacent regions, mimicking \true" motion. As the radar observes scatter from locally generated irregularities, apparent motion is equivalent to transverse motion only in the first case. The Doppler shift reveals the line of sight irregularity phase speed. Additional factors can confuse velocity measurements, such as the possibility of significant cant neutral winds (of the order 100 m/s). Nevertheless, it is tempting to assemble the apparent transverse motion and Doppler velocity information to estimate a vector velocity (perpendicular to B) Furthermore, at meter scales the predominant irregularity generation mechanism is through a streaming instability in which the velocity is approximately equal to the electron Hall drift [Schlegel, 1996], so we may also estimate a vector electric field. Data from the Super DARN HF radar is used in a similar fashion to map F region convection at high latitude [Hanuise et al., 1993]. Acknowledging the several uncertainties associated with measuring the drifts, we can at least roughly characterize the vector velocity and electric field from Doppler and interferometric drift measurements. Occasionally we can corroborate such estimates with other instruments.

For example, on 24 March, 2002, MRR detected irregularities over a period of roughly 10 hours. This extensive amount of data allowed us to make many successive interferometer measurements, each continuous over 10 seconds, spaced at intervals of 4 minutes. We measured the total velocity at several ranges in one scattering volume as it evolved over a 12 minute period (3 10-second datasets). In this particular example, the Doppler shifts were large (on the order of 800 m/s) and toward the radar; the apparent transverse drifts were relatively small (15{60 m/s). Therefore, the total irregularity drifts speeds were between 700 and 900 m/s, corresponding roughly to electric field strengths of 50{60 mV/m, which are relatively large values and indicate the disturbed ionospheric conditions under which they were measured (the K_p index during these observations was 6.0; GPS total electron content data showed depletions in the MRR field of view, indicating low conductivity and a region able to support large electric fields [Coster, 2003, private communication]). We can also estimate the direction of E by reasoning that the radar field of view is northward, so predominantly blue shifted echoes would be moving southward. With B directed \down" (into the Earth), this would mean a westward directed electric field.

4.4 Analysis of Data Products

Occasionally imperfections appear in the interferometer data products, such as phase estimates which appear organized where no target is present and coherences which exceed unity. These imperfections can be caused by ambiguities in the

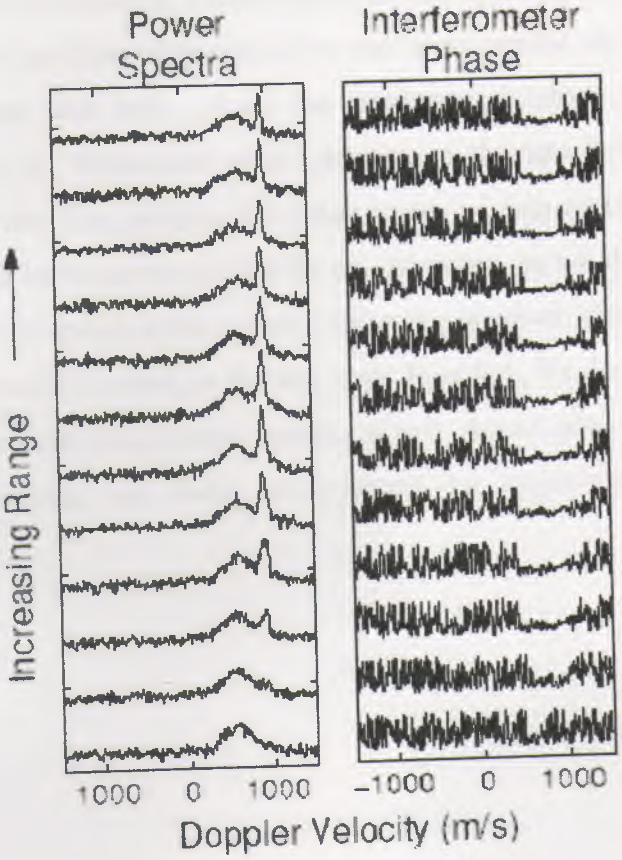

Figure 4.5 Power spectra and interferometer phase spectra over several ranges (1088-1104 km) for the 24 March 2002.

FM waveform and by the bias removal process (discussed in section 2.1). In creating the two-dimensional interferometer images, such as the one in Figure 4, we have made some simplifying assumptions. First, the azimuthal beamwidth of the interferometer is taken to be 5:6km; this value assumes 32 equally spaced lobes in a 180 degree field of view. Second, we have taken contours of constant range to be circles, which is accurate for a monostatic radar, but in our bistatic case this is an approximation. Also, while transverse size may be inferred using range information together with the 5:6km beamwidth approximation above, the transverse dimension plotted in Figures 4.4 and

4.5 remains, at best, phase information rather than a true physical dimension. Other issues concerning this azimuth aliasing were discussed earlier. Due to the very finely spaced interferometer lobes and the 4 minute wait between successive data recordings that is currently in use at MRR, it is possible that the transverse drift measurements reported in section 3.2 could be aliased by multiples of roughly 400 m/s. This is a rather large error to incur; unfortunately, experimentation with splitting the 10-second datasets into multiple parts to get finer time resolution was unsuccessful, as the variance of the phase estimates grew too large (from the necessary decrease in the number of incoherent averages) to distinguish small changes in the interferometer phase. One simple way to alleviate this problem is to take bursts of data much more often (once every minute should be frequent enough for our purposes, as we do not often observe irregularities with drift speeds greater than 1600 m/s); however, this technique was not in use during the March 24 event (or for any event thus far). We do have 2-minute-long data bursts from recent irregularity events, which would also serve to eliminate transverse drift aliasing, but these are plagued by as-yet-unsolved interference problems.

4.5 Summary

We have described the first implementation of a passive radar interferometer for volumetric targets. This new technique enables us to produce results that are functionally equivalent and comparable to those of conventional radar interferometers. We are able to form two-dimensional images of scattering volumes with very fine resolution, as well as extract geophysical properties of scatterers, such as velocity and electric field. Furthermore, with our passive system we have the advantage of reprocessing the raw data as many times as desired, with as many different settings and parameters as we wish. It is therefore possible to perform many different experiments on the same observation, allowing thorough analysis of the events we record and the possibility of making our data available in a format useful to other scientists. With the recent addition of a third antenna for collecting scattered signal, we will soon begin 10 making interferometric observations with two additional baselines, as well as with all three antennas at once, using an imaging method such as the maximum entropy method, as Hysell has done [1996], and as the radio astronomy community has demonstrated [Thompson et al., 1986]. Here, we have presented the first passive VHF radar interferometry observations of ionospheric targets. The data is of high quality, and adds to the power of passive radar as a potent tool for ionospheric radar remote sensing.

[8] L. Isserlis. On a formula for the productmoment coefficient of any order of a normal frequency distribution in any number of variables. Biometrika, 12:134{9, 1918. [9] F. D. Lind. First Passive Radar Observations of Auroral E region Irregularities. Geophys Res. Lett., 26:2155{58, 1999.

[10] M. G. Meyer. Passive VHF Radar Interferometer Implementation, Observations, and Analysis. Master's thesis, Univ. of Wash., Seattle, 2003.

4.6 Conclusions

This paper has attempted to present a review of bistatic radar systems, with particular emphasis on Passive Coherent Location (PCL) techniques. The introduction indicated that the question of whether the present interest is just another peak in the cycle will be addressed. There are several reasons why the answer to this is ‘no’, and that there is reason to believe that practical bistatic radar systems may now be developed and used. Firstly, there is ever greater spectral congestion. Military operations are likely to be carried out close to centers of population, where there are numerous broadcast and communications signals. For most purposes this spectral congestion is a problem, but for PCL it is a positive advantage. Furthermore, the VHF and UHF frequencies used by high power FM radio and television transmissions are in many senses optimum for PCL.

Secondly, as has already been pointed out, bistatic receivers are potentially simple and cheap.

Thirdly, the advent of GPS solves many of the synchronization and timing problems that have previously limited the performance of bistatic systems.

Fourthly, the inexorable increases in signal processing power mean that many of the signal digitization and processing operations are now feasible in real time. Moore’s law predicts that these advances will continue for many years. Fertile areas for new work are: (i) the use of phased array antennas and antenna signal processing techniques for ‘pulse chasing’, particularly in the context of multistatic systems, (ii) development of advanced tracking algorithms for multistatic geometries, and (iii) experimental programmers to gather bistatic clutter data, and to develop bistatic clutter models

REFERENCES

[1] D. T. Farley. Incoherent scatter correlation function measurements. Radio Sci., 4:935, 1969.

[2] D. T. Farley, H. M. Ierkic, and B. G. Fejer. Radar interferometry: A new technique for studying plasma turbulence in the ionosphere. J. Geophys. Res., 86:1467, 1981.

[3] J. M. Hansen. A new radar technique for remote sensing of atmospheric irregularities by passive observation of the scattering of commercial FM broadcasts. Master's thesis, Univ. of Wash., Seattle, 1994.

[4] C. Hanuise, C. Senior, J.-C. Cerisier, J.-P. Villain, R. A. Greenwald, J. M. Ruohoniemi, and K. B. Baker. Instantaneous mapping of high-latitude convection with coherent HF radars. J. Geophys. Res., 98:17387, 1993.

[5] J. K. Harmon. Planetary delay-Doppler radar and the long-code method. IEEE Trans. Geosci. and Remote Sensing, 40:1904, 2002.

[6] P. E. Howland. Target tracking using television-based bistatic radar. IEEE Proceedings, Radar, Sonar Navigation, 146-3:166{ 174, 1999.)

[7] D. L. Hysell. Radar imaging of equatorial F region irregularities with maximum entropy interferometry. Radio Sci., pages 1567{1578, 1996.)

[8] L. Isserlis. On a formula for the productmoment coefficient of any order of a normal frequency distribution in any number of variables. Biometrika, 12:134{9, 1918.

[9] F. D. Lind. First Passive Radar Observations of Auroral E region Irregularities. Geophys. Res. Lett., 26:2155{58, 1999.

[10] M. G. Meyer. Passive VHF Radar Interferometer Implementation, Observations, and Analysis. Master's thesis, Univ. of Wash., Seattle, 2003.

[11] M. G. Meyer, A. Morabito, and J. D. Sahr. A statistical study of high latitude ionospheric irregularity observations with VHF passive radar. In preparation.

[12] A. Morabito, M. G. Meyer, and J. D. Sahr. Improved computational performance for passive radar processing through channelizeddata. In preparation.

[13] J. F. Providakes, W. E. Swartz, D. T. Farley, and B. G. Fejer. First VHF auroral interferometer observations. Geophys. Res. Lett., 10:401, 1983.

[14] J. F. Providakes, D. T. Farley, W. E. Swartz, and D. Riggin. Plasma irregularities associated with a morning discrete auroral arc: Radar interferometer observations and theory. J. Geophys. Res., 90:7513, 1985.

[15] J. D. Sahr and F. D. Lind. The Manastash Ridge Radar: A passive bistatic radar for upper atmospheric radio science. Radio Sci., 32:2345{58, 1997.

[16] K. Schlegel. Coherent backscatter from ionospheric E-region plasma irregularities. J. Atmos. Terr. Phys., 58:933{41, 1996.

[17] A. R. Thompson, J. M. Moran, and G. W. Swenson. Interferometry and synthesis in Radio Astronomy. Wiley-Interscience, New York, 1986.

[18] Baniak, J., Baker, G., Cunningham A.M. and Martin, L., 'Silent Sentry passive surveillance', Aviation Week and Space Technology, 7 June 1999.

[19] Cherniakov, M., Nezlin, D. and Kubik, K., 'Air target detection via bistatic radar based on LEOS communication signals', IEE Proc. Radar Sonar and Navigation, Vol. 149, No. 1, pp33-38, February 2002. [20] Cherniakov, M., 'Space-surface bistatic synthetic aperture radar – prospective and problems', Proc. RADAR 2002 Conference, Edinburgh; IEE Conf. Publ. No.490, pp22–25, 15–17 October 2002.

[21] Crispin, J.W., Goodrich, R.F. and Siegel, K.M., 'A theoretical method for the calculation of the radar cross sections of aircraft and missiles', University of Michigan report 2591-1-1-M, AF 19(604)-1949, AFCRC-TN-59- 774, 1959.

[22] Davies, D. E. N., 'Use of bistatic radar techniques to improve resolution in the vertical plane', Electronics Letters., Vol.4, pp170-171, 1968.

[23] Dunsmore, M.R.B., 'Bistatic radars', chapter 11 in Advanced Radar Techniques and Systems (G. Galati ed.), Peter Peregrinus, 1993.

[24] Ewell, G.W., 'Bistatic radar cross section measurements', chapter 7 in Techniques of Radar Reflectivity Measurement, (N.C. Currie ed.), Artech House, 1989.

[25] Fawcette, J., 'Vulnerable radars seek a safe sanctuary', Microwave Systems News, April 1980, pp45-50.

[26] Griffiths, H.D., Forrest, J.R., Williams, A.D. and Pell, C., 'Digital beamforming for bistatic radar receiver'; Proc. 3rd IEE Intl. Conference on Antennas and Propagation, Norwich; IEE Conf. Publ. No. 219 Part I, pp80–84, 12–15 April 1983.

[27] Griffiths, H.D. and Carter, S.M., 'Provision of moving target indication in an independent bistatic radar receiver', The Radio and Electronic Engineer, Vol.54, No.7/8, pp336-342, July/August 1984.

[28] Griffiths, H. D., and Long, N. R W., 'Television-based bistatic radar', IEE Proceedings, Vol. 133, Part F, No.7, December 1986, pp649-657.

[29] Griffiths, H.D., Garnett, A.J., Baker, C.J. and Keaveney, S., 'Bistatic radar using satellite-borne illuminators of opportunity', Proc. RADAR-92 Conference, Brighton; IEE Conf. Publ. No.365, pp276-279, 12-13 October 1992

[30] Griffiths, H. D., Baker, C. J., Baubert, J., Kitchen, N. and Treagust, M., 'Bistatic radar using spaceborne illuminator of opportunity', Proc. RADAR 2002 Conference, Edinburgh; IEE Conf. Publ. No.490, pp1–5, 15–17 October 2002.

[31] Griffiths, H.D., Baker, C.J., Ghaleb, H., Ramakrishnan, R. and Willman, E., 'Measurement and analysis of ambiguity functions of off-air signals for passive coherent location', Electronics Letters, Vol.39, No.13, pp1005-1007, 26 June 2003.

[32] Horne, A.M. and Yates, G., 'Bistatic synthetic aperture radar', Proc. RADAR 2002 Conference, Edinburgh; IEE Conf. Publ. No.490, pp22–25, 15–17 October 2002.

[33] Howland, P. E., 'Target tracking using television-based bistatic radar', IEE Proc. Radar Sonar and Navigation, Vol. 146, No.3, June 1999, pp166-174.

[34] Jackson, M.C., 'The geometry of bistatic radar systems', IEE Proc., Vol.133, Part F., No.7, pp604-612, December 1986.

[35] Kell, R.E., 'On the derivation of bistatic RCS from monostatic measurements', Proc. IEEE, Vol.53, pp983- 988, 1965.

[36] Koch, V. and Westphal, R., 'A new approach to a multistatic passive radar sensor for air defense', Proc. IEEE International Radar Conference RADAR 2000, Washington DC, IEEE Conf. Publ No.95CH3571-0, pp22-28, 8-11 May 1995..

[37] Martinsek, D. and Goldstein, R., 'Bistatic radar experiment', Proc. EUSAR '98, European Conference on Synthetic Aperture Radar, Berlin, Germany, pp31-34, 1998.

[38] Ogrodnik, R.F., 'Broad area surveillance exploiting ambient signals via coherent techniques', Proc. IEEE International Conference on Multisensor Fusion and Integration, pp 421-429, 1004.

[39] Ogrodnik, R.F., 'Bistatic laptop radar: an affordable, silent radar alternative', Proc. IEEE National Radar Conference, Ann Arbor, MI , pp 369-373, 1996.

[40] Ogrodnik, R.F., Wolf, W.E., Schneible, R., McNamara, J., Clancy, J. and Tomlinson, P.G., 'Bistatic variants of space-based radar', Proc. IEEE Aerospace Conference, Vol.2 , pp 159-169 , 1997.

[41] Sollom, P.W., 'A little flutter on VHF', RSGB Bulletin, November 1966, pp709-728; December 1966, pp794- 824.

[42] Pell, C. and Hanle, E. (eds), Special Issue of IEE Proceedings Part F. on Bistatic Radar, IEE Proc., Vol.133, Pt.F., No.7, December 1986.

[43] Ringer, M.A. and Frazer, G.J., 'Waveform analysis of transmissions of opportunity for passive radar', Proc. ISSPA'99 , Brisbane , pp511-514 , 22-25 August 1999.
[44] Sahr, J.D. and Lind, F.D., 'The Manastash Ridge radar: a passive bistatic radar for upper atmospheric radio science ', Radio Science, Vol.32, No.6, pp2345-2358, 1977.
[45] Schoenenberger, J.G. and Forrest, J.R., 'Principles of independent receivers for use with co-operative radar transmitters ', The Radio and Electronic Engineer, Vol.52, No.2 , pp93-101, February 1982.
[46] Tsao, T., Slamani, M., Varshney, P., Weiner, D., Schwarzlander, H. and Borek, S. 'Ambiguity function for bistatic radar'; IEEE Trans. Aerospace and Electronic Systems, Vol.AES-33, pp1041-1051,1997 .
[47] Whelan, D. A., 'DISCOVERER II program summary' .